

Phenomenology of $\Lambda_b \rightarrow \Lambda_c \tau \bar{\nu}_\tau$ using lattice QCD calculations

Alakabha Datta,^{a,b} Saeed Kamali,^a Stefan Meinel,^{c,d} and Ahmed Rashed^{a,e}

^a*Department of Physics and Astronomy, University of Mississippi, Oxford, MS 38677, USA*

^b*Department of Physics and Astronomy, University of Hawaii, Honolulu, HI 96826, USA*

^c*Department of Physics, University of Arizona, Tucson, AZ 85721, USA*

^d*RIKEN BNL Research Center, Brookhaven National Laboratory, Upton, NY 11973, USA*

^e*Department of Physics, Faculty of Science, Ain Shams University, Cairo, 11566, Egypt*

E-mail: datta@phy.olemiss.edu, skamali@go.olemiss.edu,
smeinel@email.arizona.edu, amrashed@go.olemiss.edu

ABSTRACT: In a recent paper we studied the effect of new-physics operators with different Lorentz structures on the semileptonic $\Lambda_b \rightarrow \Lambda_c \tau \bar{\nu}_\tau$ decay. This decay is of interest in light of the $R(D^{(*)})$ puzzle in the semileptonic $\bar{B} \rightarrow D^{(*)} \tau \bar{\nu}_\tau$ decays. In this work we add tensor operators to extend our previous results and consider both model-independent new physics (NP) and specific classes of models proposed to address the $R(D^{(*)})$ puzzle. We show that a measurement of $R(\Lambda_c) = \mathcal{B}[\Lambda_b \rightarrow \Lambda_c \tau \bar{\nu}_\tau] / \mathcal{B}[\Lambda_b \rightarrow \Lambda_c \ell \bar{\nu}_\ell]$ can strongly constrain the NP parameters of models discussed for the $R(D^{(*)})$ puzzle. We use form factors from lattice QCD to calculate all $\Lambda_b \rightarrow \Lambda_c \tau \bar{\nu}_\tau$ observables. The $\Lambda_b \rightarrow \Lambda_c$ tensor form factors had not previously been determined in lattice QCD, and we present new lattice results for these form factors here.

Contents

1	Introduction	1
2	Formalism	4
2.1	Effective Hamiltonian	4
2.2	Decay process	5
2.2.1	Hadronic helicity amplitudes	6
2.2.2	Leptonic helicity amplitudes	9
2.3	Differential decay rate and forward-backward asymmetry	10
3	$\Lambda_b \rightarrow \Lambda_c$ tensor form factors from lattice QCD	11
4	Model-independent analysis of individual new-physics couplings	15
4.1	Constraints from the existing measurements of $R(D)$, $R(D^*)$, and τ_{B_c}	15
4.2	Impact of a future $R(\Lambda_c)$ measurement	19
5	Explicit models	22
5.1	Two-Higgs-doublet models	22
5.2	$SU(2)$ and Leptoquark models	23
6	Conclusions	36
A	Helicity spinors and polarization vectors	38
A.1	Λ_b rest frame	38
A.2	Dilepton rest frame	38

1 Introduction

A major part of particle physics research is focused on searching for physics beyond the standard model (SM). In the flavor sector a key property of the SM gauge interactions is that they are lepton flavor universal. Evidence for violation of this property would be a clear sign of new physics (NP) beyond the SM. In the search for NP, the second and third generation quarks and leptons are quite special because they are comparatively heavier and are expected to be relatively more sensitive to NP. As an example, in certain versions of the two Higgs doublet models (2HDM) the couplings of the new Higgs bosons are proportional to the masses and so NP effects are more pronounced for the heavier generations. Moreover, the constraints on new physics, especially involving the third generation leptons and quarks, are somewhat weaker allowing for larger new physics effects.

The charged-current decays $\bar{B} \rightarrow D^{(*)}\ell^-\bar{\nu}_\ell$ have been measured by the BaBar [1], Belle [2, 3] and LHCb [4] Collaborations. It is found that the values of the ratios $R(D^{(*)}) \equiv$

$\mathcal{B}(\bar{B} \rightarrow D^{(*)}\tau^-\bar{\nu}_\tau)/\mathcal{B}(\bar{B} \rightarrow D^{(*)}\ell^-\bar{\nu}_\ell)$, where $\ell = e, \mu$, considerably exceed their SM predictions.

This ratio of branching fractions has certain advantages over the absolute branching fraction measurement of $B \rightarrow D^{(*)}\tau\nu_\tau$ decays, as this is relatively less sensitive to form factor variations and several systematic uncertainties, such as those on the experimental efficiency, as well as the dependence on the value of $|V_{cb}|$, cancel in the ratio.

There are lattice QCD predictions for the ratio $R(D)_{SM}$ in the Standard Model [5–7] that are in good agreement with one another,

$$R(D)_{SM} = 0.299 \pm 0.011 \quad [\text{FNAL/MILC}], \quad (1.1)$$

$$R(D)_{SM} = 0.300 \pm 0.008 \quad [\text{HPQCD}]. \quad (1.2)$$

These values are also in good agreement with the phenomenological prediction [8]

$$R(D)_{SM} = 0.305 \pm 0.012, \quad (1.3)$$

which is based on form factors extracted from experimental data for the $B \rightarrow D\ell\bar{\nu}$ differential decay rates using heavy-quark effective theory. See also Ref. [9] for a recent analysis of $B \rightarrow D$ form factors using light-cone sum rules.

A calculation of $R(D^*)_{SM}$ is not yet available from lattice QCD. The phenomenological prediction using form factors extracted from $B \rightarrow D^*\ell\bar{\nu}$ experimental data is [10]

$$R(D^*)_{SM} = 0.252 \pm 0.003. \quad (1.4)$$

The averages of $R(D)$ and $R(D^*)$ measurements, evaluated by the Heavy-Flavor Averaging Group, are [11]

$$R(D)_{exp} = 0.397 \pm 0.040 \pm 0.028, \quad (1.5)$$

$$R(D^*)_{exp} = 0.316 \pm 0.016 \pm 0.010, \quad (1.6)$$

where the first uncertainty is statistical and the second is systematic. $R(D^*)$ and $R(D)$ exceed the SM predictions by 3.3σ and 1.9σ , respectively. The combined analysis of $R(D^*)$ and $R(D)$, taking into account measurement correlations, finds that the deviation is 4σ from the SM prediction [11, 12].

Since lattice QCD results are not yet available for the $B \rightarrow D^*$ form factors at nonzero recoil and for the $B \rightarrow D$ tensor form factor, we use the phenomenological form factors from Ref. [8] for both channels in our analysis. For $B \rightarrow D$, we have compared the phenomenological results for f_0 and f_+ to the results obtained from a joint BGL z -expansion fit [13] to the FNAL/MILC lattice QCD results [6] and Babar [14] and Belle experimental data [15], and we found that the differences between both sets of form factors are below 5% across the entire kinematic range. The constraints on the new-physics couplings from the experimental measurement of $R(D)$ obtained with both sets of form factors are practically identical.

We also construct the ratios of the experimental results (1.5) and (1.6) to the phenomenological SM predictions (1.3) and (1.4):

$$R_D^{Ratio} = \frac{R(D)_{exp}}{R(D)_{SM}} = 1.30 \pm 0.17, \quad (1.7)$$

$$R_{D^*}^{Ratio} = \frac{R(D^*)_{exp}}{R(D^*)_{SM}} = 1.25 \pm 0.08. \quad (1.8)$$

There have been numerous analyses examining NP explanations of the $R(D^{(*)})$ measurements [8, 16–31]. The new physics involves new charged-current interactions. In the neutral-current sector, data from $b \rightarrow s\ell^+\ell^-$ decays also hint at lepton flavor non-universality – the so called R_K puzzle: the LHCb Collaboration has found a 2.6σ deviation from the SM prediction for the ratio $R_K \equiv \mathcal{B}(B^+ \rightarrow K^+\mu^+\mu^-)/\mathcal{B}(B^+ \rightarrow K^+e^+e^-)$ in the dilepton invariant mass-squared range $1 \text{ GeV}^2 \leq q^2 \leq 6 \text{ GeV}^2$ [32]. There are also other, not necessarily lepton-flavor non-universal anomalies in $b \rightarrow s\ell^+\ell^-$ decays, most significantly in the $B^0 \rightarrow K^{*0}\mu^+\mu^-$ angular observable P'_5 [33, 34]. Global fits of the experimental data prefer a negative shift in one of the $b \rightarrow s\mu^+\mu^-$ Wilson coefficients, C_9 [35]. Common explanations of the $b \rightarrow c\tau^-\bar{\nu}_\tau$ and $b \rightarrow s\mu^+\mu^-$ anomalies have been proposed in Refs. [31, 36–40].

The underlying quark level transition $b \rightarrow c\tau^-\bar{\nu}_\tau$ in the $R(D^{(*)})$ puzzle can be probed in both B and Λ_b decays. Recently, the decay $\Lambda_b \rightarrow \Lambda_c\tau\bar{\nu}_\tau$ was discussed in the standard model and with new physics in Ref. [41–47]. $\Lambda_b \rightarrow \Lambda_c\tau\bar{\nu}_\tau$ decays could be useful to confirm possible new physics in the $R(D^{(*)})$ puzzle and to point to the correct model of new physics.

In Ref. [43] the following quantities were calculated within the SM and with various new physics operators:

$$R(\Lambda_c) = \frac{\mathcal{B}[\Lambda_b \rightarrow \Lambda_c\tau\bar{\nu}_\tau]}{\mathcal{B}[\Lambda_b \rightarrow \Lambda_c\ell\bar{\nu}_\ell]} \quad (1.9)$$

and

$$B_{\Lambda_c}(q^2) = \frac{\frac{d\Gamma[\Lambda_b \rightarrow \Lambda_c\tau\bar{\nu}_\tau]}{dq^2}}{\frac{d\Gamma[\Lambda_b \rightarrow \Lambda_c\ell\bar{\nu}_\ell]}{dq^2}}, \quad (1.10)$$

where ℓ represents μ or e . In this paper we work with the ratio $R_{\Lambda_c}^{Ratio}$, defined as

$$R_{\Lambda_c}^{Ratio} = \frac{R(\Lambda_c)^{SM+NP}}{R(\Lambda_c)^{SM}}. \quad (1.11)$$

We also consider the forward-backward asymmetry

$$A_{FB}(q^2) = \frac{\int_0^1 (d^2\Gamma/dq^2 d\cos\theta_\tau) d\cos\theta_\tau - \int_{-1}^0 (d^2\Gamma/dq^2 d\cos\theta_\tau) d\cos\theta_\tau}{d\Gamma/dq^2}, \quad (1.12)$$

where θ_τ is the angle between the momenta of the τ lepton and Λ_c baryon in the dilepton rest frame.

This paper improves upon the earlier work [43] in several ways:

- We add tensor interactions in the effective Lagrangian.
- Instead of a quark model, we use form factors from lattice QCD to calculate all $\Lambda_b \rightarrow \Lambda_c \tau \bar{\nu}_\tau$ observable. The vector and axial vector form factors are taken from Ref. [48], and we extend the analysis of Ref. [48] to obtain lattice QCD results for the tensor form factors as well.
- In addition to $R(\Lambda_c)$ and $B_{\Lambda_c}(q^2)$, we also calculate the forward-backward asymmetry (1.12) in the SM and with new physics.
- We include new constraints from the B_c lifetime [47, 49, 50] in our analysis.
- In addition to analyzing the effects of individual new physics-couplings, we study specific models that introduce multiple new-physics couplings simultaneously. We consider a 2-Higgs doublet model, models with new vector bosons, and several lepto-quark models.

The paper is organized in the following manner: In Sec. 2 we introduce the effective Lagrangian to parametrize the NP operators and give the expressions for the decay distribution in terms of helicity amplitudes. In Sec. 3, we present the new lattice QCD results for the tensor form factors. The model-independent phenomenological analysis of individual new-physics couplings is discussed in Sec. 4, while explicit models are considered in Sec. 5. We conclude in Sec. 6.

2 Formalism

2.1 Effective Hamiltonian

In the presence of NP, the effective Hamiltonian for the quark-level transition $b \rightarrow c \tau^- \bar{\nu}_\tau$ can be written in the form [51, 52]

$$\begin{aligned} \mathcal{H}_{eff} = \frac{G_F V_{cb}}{\sqrt{2}} \bigg\{ & \left[\bar{c} \gamma_\mu (1 - \gamma_5) b + g_L \bar{c} \gamma_\mu (1 - \gamma_5) b + g_R \bar{c} \gamma_\mu (1 + \gamma_5) b \right] \bar{\tau} \gamma^\mu (1 - \gamma_5) \nu_\tau \\ & + \left[g_S \bar{c} b + g_P \bar{c} \gamma_5 b \right] \bar{\tau} (1 - \gamma_5) \nu_\tau + \left[g_T \bar{c} \sigma^{\mu\nu} (1 - \gamma_5) b \right] \bar{\tau} \sigma_{\mu\nu} (1 - \gamma_5) \nu_\tau + h.c. \bigg\}, \end{aligned} \quad (2.1)$$

where G_F is the Fermi constant, V_{cb} is the Cabibbo-Kobayashi-Maskawa (CKM) matrix element, and we use $\sigma_{\mu\nu} = i[\gamma_\mu, \gamma_\nu]/2$. We consider that the above Hamiltonian is written at the m_b energy scale.

If the effective interaction is written at the cut-off scale Λ then running down to the m_b scale will generate new operators and new contributions, which have been discussed in Refs. [53, 54]. These new contributions can strongly constrain models but to really calculate their true impacts we have to consider specific models where there might be cancellations between various terms.

The SM effective Hamiltonian corresponds to $g_L = g_R = g_S = g_P = g_T = 0$. In Eq. (2.1), we have assumed the neutrinos to be always left chiral. In general, with NP the

neutrino associated with the τ lepton does not have to carry the same flavor. In the model-independent analysis of individual couplings (Sec. 4) we will not consider this possibility. Specific models will be discussed in Sec. 5.

2.2 Decay process

The process under consideration is

$$\Lambda_b(p_{\Lambda_b}) \rightarrow \tau^-(p_\tau) + \bar{\nu}_\tau(p_{\bar{\nu}_\tau}) + \Lambda_c(p_{\Lambda_c}).$$

The differential decay rate for this process can be represented as [23]

$$\frac{d\Gamma}{dq^2 d\cos\theta_\tau} = \frac{G_F^2 |V_{cb}|^2}{2048\pi^3} \left(1 - \frac{m_\tau^2}{q^2}\right) \frac{\sqrt{Q_+ Q_-}}{m_{\Lambda_b}^3} \sum_{\lambda_{\Lambda_c}} \sum_{\lambda_\tau} |\mathcal{M}_{\lambda_{\Lambda_c}}^{\lambda_\tau}|^2, \quad (2.2)$$

where

$$q = p_{\Lambda_b} - p_{\Lambda_c}, \quad (2.3)$$

$$Q_\pm = (m_{\Lambda_b} \pm m_{\Lambda_c})^2 - q^2, \quad (2.4)$$

and the helicity amplitude $\mathcal{M}_{\lambda_{\Lambda_c}}^{\lambda_\tau}$ is written as

$$\mathcal{M}_{\lambda_{\Lambda_c}}^{\lambda_\tau} = H_{\lambda_{\Lambda_c}, \lambda_\tau=0}^{SP} + \sum_{\lambda} \eta_{\lambda} H_{\lambda_{\Lambda_c}, \lambda}^{VA} L_{\lambda}^{\lambda_\tau} + \sum_{\lambda, \lambda'} \eta_{\lambda} \eta_{\lambda'} H_{\lambda_{\Lambda_c}, \lambda, \lambda'}^{(T)\lambda_{\Lambda_b}} L_{\lambda, \lambda'}^{\lambda_\tau}. \quad (2.5)$$

Here, (λ, λ') indicate the helicity of the virtual vector boson (see Appendix A), λ_{Λ_c} and λ_τ are the helicities of the Λ_c baryon and τ lepton, respectively, and $\eta_{\lambda} = 1$ for $\lambda = t$ and $\eta_{\lambda} = -1$ for $\lambda = 0, \pm 1$.

The scalar-type, vector/axial-vector-type, and tensor-type hadronic helicity amplitudes are defined as

$$\begin{aligned} H_{\lambda_{\Lambda_c}, \lambda=0}^{SP} &= H_{\lambda_{\Lambda_c}, \lambda=0}^S + H_{\lambda_{\Lambda_c}, \lambda=0}^P, \\ H_{\lambda_{\Lambda_c}, \lambda=0}^S &= g_S \langle \Lambda_c | \bar{c}b | \Lambda_b \rangle, \\ H_{\lambda_{\Lambda_c}, \lambda=0}^P &= g_P \langle \Lambda_c | \bar{c}\gamma_5 b | \Lambda_b \rangle, \end{aligned} \quad (2.6)$$

$$\begin{aligned} H_{\lambda_{\Lambda_c}, \lambda}^{VA} &= H_{\lambda_{\Lambda_c}, \lambda}^V - H_{\lambda_{\Lambda_c}, \lambda}^A, \\ H_{\lambda_{\Lambda_c}, \lambda}^V &= (1 + g_L + g_R) \epsilon^{*\mu}(\lambda) \langle \Lambda_c | \bar{c}\gamma_\mu b | \Lambda_b \rangle, \\ H_{\lambda_{\Lambda_c}, \lambda}^A &= (1 + g_L - g_R) \epsilon^{*\mu}(\lambda) \langle \Lambda_c | \bar{c}\gamma_\mu \gamma_5 b | \Lambda_b \rangle, \end{aligned} \quad (2.7)$$

and

$$\begin{aligned} H_{\lambda_{\Lambda_c}, \lambda, \lambda'}^{(T)\lambda_{\Lambda_b}} &= H_{\lambda_{\Lambda_c}, \lambda, \lambda'}^{(T1)\lambda_{\Lambda_b}} - H_{\lambda_{\Lambda_c}, \lambda, \lambda'}^{(T2)\lambda_{\Lambda_b}}, \\ H_{\lambda_{\Lambda_c}, \lambda, \lambda'}^{(T1)\lambda_{\Lambda_b}} &= g_T \epsilon^{*\mu}(\lambda) \epsilon^{*\nu}(\lambda') \langle \Lambda_c | \bar{c}i\sigma_{\mu\nu} b | \Lambda_b \rangle, \\ H_{\lambda_{\Lambda_c}, \lambda, \lambda'}^{(T2)\lambda_{\Lambda_b}} &= g_T \epsilon^{*\mu}(\lambda) \epsilon^{*\nu}(\lambda') \langle \Lambda_c | \bar{c}i\sigma_{\mu\nu} \gamma_5 b | \Lambda_b \rangle. \end{aligned} \quad (2.8)$$

The leptonic amplitudes are defined as

$$\begin{aligned}
L^{\lambda_\tau} &= \langle \tau \bar{\nu}_\tau | \bar{\tau} (1 - \gamma_5) \nu_\tau | 0 \rangle, \\
L_\lambda^{\lambda_\tau} &= \epsilon^\mu(\lambda) \langle \tau \bar{\nu}_\tau | \bar{\tau} \gamma_\mu (1 - \gamma_5) \nu_\tau | 0 \rangle, \\
L_{\lambda, \lambda'}^{\lambda_\tau} &= -i \epsilon^\mu(\lambda) \epsilon^\nu(\lambda') \langle \tau \bar{\nu}_\tau | \bar{\tau} \sigma_{\mu\nu} (1 - \gamma_5) \nu_\tau | 0 \rangle.
\end{aligned} \tag{2.9}$$

Above, ϵ^μ are the polarization vectors of the virtual vector boson (see Appendix A). The explicit expressions for the hadronic and leptonic helicity amplitudes are presented in the following.

2.2.1 Hadronic helicity amplitudes

In this paper, we use the helicity-based definition of the $\Lambda_b \rightarrow \Lambda_c$ form factors, which was introduced in [55]. The matrix elements of the vector and axial vector currents can be written in terms of six helicity form factors F_+ , F_\perp , F_0 , G_+ , G_\perp , and G_0 as follows:

$$\begin{aligned}
\langle \Lambda_c | \bar{c} \gamma^\mu b | \Lambda_b \rangle &= \bar{u}_{\Lambda_c} \left[F_0(q^2) (m_{\Lambda_b} - m_{\Lambda_c}) \frac{q^\mu}{q^2} \right. \\
&\quad + F_+(q^2) \frac{m_{\Lambda_b} + m_{\Lambda_c}}{Q_+} (p_{\Lambda_b}^\mu + p_{\Lambda_c}^\mu - (m_{\Lambda_b}^2 - m_{\Lambda_c}^2) \frac{q^\mu}{q^2}) \\
&\quad \left. + F_\perp(q^2) (\gamma^\mu - \frac{2m_{\Lambda_c}}{Q_+} p_{\Lambda_b}^\mu - \frac{2m_{\Lambda_b}}{Q_+} p_{\Lambda_c}^\mu) \right] u_{\Lambda_b},
\end{aligned} \tag{2.10}$$

$$\begin{aligned}
\langle \Lambda_c | \bar{c} \gamma^\mu \gamma_5 b | \Lambda_b \rangle &= -\bar{u}_{\Lambda_c} \gamma_5 \left[G_0(q^2) (m_{\Lambda_b} + m_{\Lambda_c}) \frac{q^\mu}{q^2} \right. \\
&\quad + G_+(q^2) \frac{m_{\Lambda_b} - m_{\Lambda_c}}{Q_-} (p_{\Lambda_b}^\mu + p_{\Lambda_c}^\mu - (m_{\Lambda_b}^2 - m_{\Lambda_c}^2) \frac{q^\mu}{q^2}) \\
&\quad \left. + G_\perp(q^2) (\gamma^\mu + \frac{2m_{\Lambda_c}}{Q_-} p_{\Lambda_b}^\mu - \frac{2m_{\Lambda_b}}{Q_-} p_{\Lambda_c}^\mu) \right] u_{\Lambda_b}.
\end{aligned} \tag{2.11}$$

The matrix elements of the scalar and pseudoscalar currents can be obtained from the vector and axial vector matrix elements using the equations of motion:

$$\begin{aligned}
\langle \Lambda_c | \bar{c} b | \Lambda_b \rangle &= \frac{q_\mu}{m_b - m_c} \langle \Lambda_c | \bar{c} \gamma^\mu b | \Lambda_b \rangle \\
&= F_0(q^2) \frac{m_{\Lambda_b} - m_{\Lambda_c}}{m_b - m_c} \bar{u}_{\Lambda_c} u_{\Lambda_b},
\end{aligned} \tag{2.12}$$

$$\begin{aligned}
\langle \Lambda_c | \bar{c} \gamma_5 b | \Lambda_b \rangle &= \frac{q_\mu}{m_b + m_c} \langle \Lambda_c | \bar{c} \gamma^\mu \gamma_5 b | \Lambda_b \rangle \\
&= G_0(q^2) \frac{m_{\Lambda_b} + m_{\Lambda_c}}{m_b + m_c} \bar{u}_{\Lambda_c} \gamma_5 u_{\Lambda_b}.
\end{aligned} \tag{2.13}$$

In our numerical analysis, we use $m_b = 4.18(4)$ GeV, $m_c = 1.27(3)$ GeV [56]. The matrix elements of the tensor currents can be written in terms of four form factors h_+ , h_\perp , \tilde{h}_+ ,

\tilde{h}_\perp ,

$$\begin{aligned}
\langle \Lambda_c | \bar{c} i \sigma^{\mu\nu} b | \Lambda_b \rangle = & \bar{u}_{\Lambda_c} \left[2h_+(q^2) \frac{p_{\Lambda_b}^\mu p_{\Lambda_c}^\nu - p_{\Lambda_b}^\nu p_{\Lambda_c}^\mu}{Q_+} \right. \\
& + h_\perp(q^2) \left(\frac{m_{\Lambda_b} + m_{\Lambda_c}}{q^2} (q^\mu \gamma^\nu - q^\nu \gamma^\mu) - 2 \left(\frac{1}{q^2} + \frac{1}{Q_+} \right) (p_{\Lambda_b}^\mu p_{\Lambda_c}^\nu - p_{\Lambda_b}^\nu p_{\Lambda_c}^\mu) \right) \\
& + \tilde{h}_+(q^2) \left(i \sigma^{\mu\nu} - \frac{2}{Q_-} (m_{\Lambda_b} (p_{\Lambda_c}^\mu \gamma^\nu - p_{\Lambda_c}^\nu \gamma^\mu) \right. \\
& \left. - m_{\Lambda_c} (p_{\Lambda_b}^\mu \gamma^\nu - p_{\Lambda_b}^\nu \gamma^\mu) + p_{\Lambda_b}^\mu p_{\Lambda_c}^\nu - p_{\Lambda_b}^\nu p_{\Lambda_c}^\mu) \right) \\
& + \tilde{h}_\perp(q^2) \frac{m_{\Lambda_b} - m_{\Lambda_c}}{q^2 Q_-} \left((m_{\Lambda_b}^2 - m_{\Lambda_c}^2 - q^2) (\gamma^\mu p_{\Lambda_b}^\nu - \gamma^\nu p_{\Lambda_b}^\mu) \right. \\
& \left. \left. - (m_{\Lambda_b}^2 - m_{\Lambda_c}^2 + q^2) (\gamma^\mu p_{\Lambda_c}^\nu - \gamma^\nu p_{\Lambda_c}^\mu) + 2(m_{\Lambda_b} - m_{\Lambda_c}) (p_{\Lambda_b}^\mu p_{\Lambda_c}^\nu - p_{\Lambda_b}^\nu p_{\Lambda_c}^\mu) \right) \right] u_{\Lambda_b}.
\end{aligned} \tag{2.14}$$

The matrix elements of the current $\bar{c} i \sigma^{\mu\nu} \gamma_5 b$ can be obtained from the above equation by using the identity

$$\sigma^{\mu\nu} \gamma_5 = -\frac{i}{2} \epsilon^{\mu\nu\alpha\beta} \sigma_{\alpha\beta}. \tag{2.15}$$

In the following, only the non-vanishing helicity amplitudes are given. The scalar and pseudo-scalar helicity amplitudes associated with the new physics scalar and pseudo-scalar interactions are

$$H_{1/2,0}^{SP} = F_0 g_S \frac{\sqrt{Q_+}}{m_b - m_c} (m_{\Lambda_b} - m_{\Lambda_c}) - G_0 g_P \frac{\sqrt{Q_-}}{m_b + m_c} (m_{\Lambda_b} + m_{\Lambda_c}), \tag{2.16}$$

$$H_{-1/2,0}^{SP} = F_0 g_S \frac{\sqrt{Q_+}}{m_b - m_c} (m_{\Lambda_b} - m_{\Lambda_c}) + G_0 g_P \frac{\sqrt{Q_-}}{m_b + m_c} (m_{\Lambda_b} + m_{\Lambda_c}). \tag{2.17}$$

The parity-related amplitudes are

$$\begin{aligned}
H_{\lambda_{\Lambda_c}, \lambda_{NP}}^S &= H_{-\lambda_{\Lambda_c}, -\lambda_{NP}}^S, \\
H_{\lambda_{\Lambda_c}, \lambda_{NP}}^P &= -H_{-\lambda_{\Lambda_c}, -\lambda_{NP}}^P.
\end{aligned} \tag{2.18}$$

For the vector and axial-vector helicity amplitudes, we find

$$\begin{aligned}
H_{1/2,0}^{VA} &= F_+(1 + g_L + g_R) \frac{\sqrt{Q_-}}{\sqrt{q^2}} (m_{\Lambda_b} + m_{\Lambda_c}) \\
&\quad - G_+(1 + g_L - g_R) \frac{\sqrt{Q_+}}{\sqrt{q^2}} (m_{\Lambda_b} - m_{\Lambda_c}), \tag{2.19}
\end{aligned}$$

$$H_{1/2,+1}^{VA} = -F_\perp(1 + g_L + g_R) \sqrt{2Q_-} + G_\perp(1 + g_L - g_R) \sqrt{2Q_+}, \tag{2.20}$$

$$\begin{aligned}
H_{1/2,t}^{VA} &= F_0(1 + g_L + g_R) \frac{\sqrt{Q_+}}{\sqrt{q^2}} (m_{\Lambda_b} - m_{\Lambda_c}) \\
&\quad - G_0(1 + g_L - g_R) \frac{\sqrt{Q_-}}{\sqrt{q^2}} (m_{\Lambda_b} + m_{\Lambda_c}), \tag{2.21}
\end{aligned}$$

$$\begin{aligned}
H_{-1/2,0}^{VA} &= F_+(1 + g_L + g_R) \frac{\sqrt{Q_-}}{\sqrt{q^2}} (m_{\Lambda_b} + m_{\Lambda_c}) \\
&\quad + G_+(1 + g_L - g_R) \frac{\sqrt{Q_+}}{\sqrt{q^2}} (m_{\Lambda_b} - m_{\Lambda_c}), \tag{2.22}
\end{aligned}$$

$$H_{-1/2,-1}^{VA} = -F_\perp(1 + g_L + g_R) \sqrt{2Q_-} - G_\perp(1 + g_L - g_R) \sqrt{2Q_+}, \tag{2.23}$$

$$\begin{aligned}
H_{-1/2,t}^{VA} &= F_0(1 + g_L + g_R) \frac{\sqrt{Q_+}}{\sqrt{q^2}} (m_{\Lambda_b} - m_{\Lambda_c}) \\
&\quad + G_0(1 + g_L - g_R) \frac{\sqrt{Q_-}}{\sqrt{q^2}} (m_{\Lambda_b} + m_{\Lambda_c}). \tag{2.24}
\end{aligned}$$

We also have the relations

$$\begin{aligned}
H_{\lambda_{\Lambda_c}, \lambda_w}^V &= H_{-\lambda_{\Lambda_c}, -\lambda_w}^V, \\
H_{\lambda_{\Lambda_c}, \lambda_w}^A &= -H_{-\lambda_{\Lambda_c}, -\lambda_w}^A. \tag{2.25}
\end{aligned}$$

The tensor helicity amplitudes are

$$H_{-1/2,t,0}^{(T)-1/2} = -g_T \left[-h_+ \sqrt{Q_-} + \tilde{h}_+ \sqrt{Q_+} \right], \quad (2.26)$$

$$H_{+1/2,t,0}^{(T)+1/2} = g_T \left[h_+ \sqrt{Q_-} + \tilde{h}_+ \sqrt{Q_+} \right], \quad (2.27)$$

$$H_{+1/2,t,+1}^{(T)-1/2} = -g_T \frac{\sqrt{2}}{\sqrt{q^2}} \left[h_\perp (m_{\Lambda_b} + m_{\Lambda_c}) \sqrt{Q_-} + \tilde{h}_\perp (m_{\Lambda_b} - m_{\Lambda_c}) \sqrt{Q_+} \right], \quad (2.28)$$

$$H_{-1/2,t,-1}^{(T)+1/2} = -g_T \frac{\sqrt{2}}{\sqrt{q^2}} \left[h_\perp (m_{\Lambda_b} + m_{\Lambda_c}) \sqrt{Q_-} - \tilde{h}_\perp (m_{\Lambda_b} - m_{\Lambda_c}) \sqrt{Q_+} \right], \quad (2.29)$$

$$H_{+1/2,0,+1}^{(T)-1/2} = -g_T \frac{\sqrt{2}}{\sqrt{q^2}} \left[h_\perp (m_{\Lambda_b} + m_{\Lambda_c}) \sqrt{Q_-} + \tilde{h}_\perp (m_{\Lambda_b} - m_{\Lambda_c}) \sqrt{Q_+} \right], \quad (2.30)$$

$$H_{-1/2,0,-1}^{(T)+1/2} = g_T \frac{\sqrt{2}}{\sqrt{q^2}} \left[h_\perp (m_{\Lambda_b} + m_{\Lambda_c}) \sqrt{Q_-} - \tilde{h}_\perp (m_{\Lambda_b} - m_{\Lambda_c}) \sqrt{Q_+} \right], \quad (2.31)$$

$$H_{+1/2,+1,-1}^{(T)+1/2} = -g_T \left[h_+ \sqrt{Q_-} + \tilde{h}_+ \sqrt{Q_+} \right], \quad (2.32)$$

$$H_{-1/2,+1,-1}^{(T)-1/2} = -g_T \left[h_+ \sqrt{Q_-} - \tilde{h}_+ \sqrt{Q_+} \right]. \quad (2.33)$$

The other non-vanishing helicity amplitudes of tensor type are related to the above by

$$H_{\lambda_{\Lambda_c}, \lambda, \lambda'}^{(T)\lambda_{\Lambda_b}} = -H_{\lambda_{\Lambda_c}, \lambda', \lambda}^{(T)\lambda_{\Lambda_b}}. \quad (2.34)$$

2.2.2 Leptonic helicity amplitudes

In the following, we define

$$v = \sqrt{1 - \frac{m_\tau^2}{q^2}}. \quad (2.35)$$

The scalar and pseudoscalar leptonic helicity amplitudes are

$$L^{+1/2} = 2\sqrt{q^2}v, \quad (2.36)$$

$$L^{-1/2} = 0, \quad (2.37)$$

the vector and axial-vector amplitudes are

$$L_{\pm 1}^{+1/2} = \pm \sqrt{2} m_\tau v \sin(\theta_\tau), \quad (2.38)$$

$$L_0^{+1/2} = -2m_\tau v \cos(\theta_\tau), \quad (2.39)$$

$$L_t^{+1/2} = 2m_\tau v, \quad (2.40)$$

$$L_{\pm 1}^{-1/2} = \sqrt{2q^2}v (1 \pm \cos(\theta_\tau)), \quad (2.41)$$

$$L_0^{-1/2} = 2\sqrt{q^2}v \sin(\theta_\tau), \quad (2.42)$$

$$L_t^{-1/2} = 0, \quad (2.43)$$

and the tensor amplitudes are

$$L_{0,\pm 1}^{+1/2} = -\sqrt{2q^2}v \sin(\theta_\tau), \quad (2.44)$$

$$L_{\pm 1,t}^{+1/2} = \mp \sqrt{2q^2}v \sin(\theta_\tau), \quad (2.45)$$

$$L_{t,0}^{+1/2} = L_{+1,-1}^{+1/2} = -2\sqrt{q^2}v \cos(\theta_\tau), \quad (2.46)$$

$$L_{0,\pm 1}^{-1/2} = \mp \sqrt{2}m_\tau v (1 \pm \cos(\theta_\tau)), \quad (2.47)$$

$$L_{\pm 1,t}^{-1/2} = -\sqrt{2}m_\tau v (1 \pm \cos(\theta_\tau)), \quad (2.48)$$

$$L_{t,0}^{-1/2} = L_{+1,-1}^{-1/2} = 2m_\tau v \sin(\theta_\tau). \quad (2.49)$$

Here we have the relation

$$L_{\lambda,\lambda'}^{\lambda_\tau} = -L_{\lambda',\lambda}^{\lambda_\tau}. \quad (2.50)$$

The angle θ_τ is defined as the angle between the momenta of the τ lepton and Λ_c baryon in the dilepton rest frame.

2.3 Differential decay rate and forward-backward asymmetry

From the twofold decay distribution (2.2), we obtain the following expression for the differential decay rate by integrating over $\cos \theta_\tau$:

$$\begin{aligned} \frac{d\Gamma(\Lambda_b \rightarrow \Lambda_c \tau \bar{\nu}_\tau)}{dq^2} &= \frac{G_F^2 |V_{cb}|^2}{384\pi^3} \frac{q^2 \sqrt{Q_+ Q_-}}{m_{\Lambda_b}^3} \left(1 - \frac{m_\tau^2}{q^2}\right)^2 \left[A_1^{VA} + \frac{m_\tau^2}{2q^2} A_2^{VA} + \frac{3}{2} A_3^{SP} \right. \\ &\quad \left. + 2\left(1 + \frac{2m_\tau^2}{q^2}\right) A_4^T + \frac{3m_\tau}{\sqrt{q^2}} A_5^{VA-SP} + \frac{6m_\tau}{\sqrt{q^2}} A_6^{VA-T} \right], \end{aligned} \quad (2.51)$$

where

$$\begin{aligned} A_1^{VA} &= |H_{1/2,1}^{VA}|^2 + |H_{1/2,0}^{VA}|^2 + |H_{-1/2,0}^{VA}|^2 + |H_{-1/2,-1}^{VA}|^2, \\ A_2^{VA} &= |H_{1/2,1}^{VA}|^2 + |H_{1/2,0}^{VA}|^2 + |H_{-1/2,0}^{VA}|^2 + |H_{-1/2,-1}^{VA}|^2 + 3|H_{1/2,t}^{VA}|^2 + 3|H_{-1/2,t}^{VA}|^2, \\ A_3^{SP} &= |H_{1/2,0}^{SP}|^2 + |H_{-1/2,0}^{SP}|^2, \\ A_4^T &= |H_{1/2,t,0}^{(T)1/2} + H_{1/2,-1,1}^{(T)1/2}|^2 + |H_{-1/2,t,-1}^{(T)1/2} + H_{-1/2,-1,0}^{(T)1/2}|^2 + |H_{1/2,0,1}^{(T)-1/2} + H_{1/2,t,1}^{(T)-1/2}|^2 \\ &\quad + |H_{-1/2,-1,1}^{(T)-1/2} + H_{-1/2,t,0}^{(T)-1/2}|^2, \\ A_5^{VA-SP} &= \text{Re}(H_{1/2,0}^{SP*} H_{1/2,t}^{VA} + H_{-1/2,0}^{SP*} H_{-1/2,t}^{VA}), \\ A_6^{VA-T} &= \text{Re}[H_{1/2,0}^{VA*} (H_{1/2,-1,1}^{(T)1/2} + H_{1/2,t,0}^{(T)1/2})] + \text{Re}[H_{1/2,1}^{VA*} (H_{1/2,0,1}^{(T)-1/2} + H_{1/2,t,1}^{(T)-1/2})] + \\ &\quad \text{Re}[H_{-1/2,0}^{VA*} (H_{-1/2,-1,1}^{(T)-1/2} + H_{-1/2,t,0}^{(T)-1/2})] + \text{Re}[H_{-1/2,-1}^{VA*} (H_{-1/2,-1,0}^{(T)1/2} + H_{-1/2,t,-1}^{(T)1/2})]. \end{aligned} \quad (2.52)$$

Here, A_1^{VA} and A_2^{VA} are the (axial-)vector non-spin-flip and spin-flip terms respectively, A_3^{SP} and A_4^T are the pure (pseudo-)scalar and tensor terms respectively; and A_5^{VA-SP} and A_6^{VA-T} are interference terms. The scalar-tensor interference term is proportional to $\cos \theta_\tau$ and vanishes after integration over $\cos \theta_\tau$.

For the forward-backward asymmetry (1.12) we have

$$A_{FB}(q^2) = \left(\frac{d\Gamma}{dq^2} \right)^{-1} \frac{G_F^2 V_{cb}^2 q^2 \sqrt{Q_+ Q_-}}{512 \pi^3 m_{\Lambda_b}^3} \left(1 - \frac{m_\tau^2}{q^2} \right)^2 \left[B_1^{VA} + \frac{2m_\tau^2}{q^2} B_2^{VA} + \frac{4m_\tau^2}{q^2} B_3^T + \right. \\ \left. \frac{2m_\tau}{\sqrt{q^2}} B_4^{VA-SP} + \frac{4m_\tau}{\sqrt{q^2}} B_5^{VA-T} + 4B_6^{SP-T} \right], \quad (2.53)$$

where

$$B_1^{VA} = |H_{1/2,1}^{VA}|^2 - |H_{-1/2,-1}^{VA}|^2, \\ B_2^{VA} = \text{Re}[H_{1/2,t}^{VA*} H_{1/2,0}^{VA} + H_{-1/2,t}^{VA*} H_{-1/2,0}^{VA}], \\ B_3^T = |H_{1/2,0,1}^{(T)-1/2} + H_{1/2,t,1}^{(T)-1/2}|^2 - |H_{-1/2,-1,0}^{(T)1/2} + H_{-1/2,t,-1}^{(T)1/2}|^2, \\ B_4^{VA-SP} = \text{Re}[H_{1/2,0}^{SP*} H_{1/2,0}^{VA} + H_{-1/2,0}^{SP*} H_{-1/2,0}^{VA}], \\ B_5^{VA-T} = \text{Re}[H_{1/2,t}^{VA*} (H_{1/2,-1,1}^{(T)1/2} + H_{1/2,t,0}^{(T)1/2})] + \text{Re}[H_{1/2,1}^{VA*} (H_{1/2,0,1}^{(T)-1/2} + H_{1/2,t,1}^{(T)-1/2})] \\ + \text{Re}[H_{-1/2,t}^{VA*} (H_{-1/2,-1,1}^{(T)-1/2} + H_{-1/2,t,0}^{(T)-1/2})] - \text{Re}[H_{-1/2,-1}^{VA*} (H_{-1/2,-1,0}^{(T)1/2} + H_{-1/2,t,-1}^{(T)1/2})], \\ B_6^{SP-T} = \text{Re}[H_{1/2,0}^{SP*} (H_{1/2,-1,1}^{(T)1/2} + H_{1/2,t,0}^{(T)1/2})] + \text{Re}[H_{-1/2,0}^{SP*} (H_{-1/2,-1,1}^{(T)-1/2} + H_{-1/2,t,0}^{(T)-1/2})]. \quad (2.54)$$

There is no contribution from pure (pseudo-)scalar operators to the forward-backward asymmetry, but all possible interference terms are present.

3 $\Lambda_b \rightarrow \Lambda_c$ tensor form factors from lattice QCD

This work uses $\Lambda_b \rightarrow \Lambda_c$ form factors computed in lattice QCD. The vector and axial vector form factors defined in Eqs. (2.10) and (2.11) are taken from Ref. [48]. For the purposes of the present work, one of us (SM) extended the analysis of Ref. [48] to include the tensor form factors defined in Eq. (2.14). The tensor form factors were extracted from the lattice QCD correlation functions using ratios defined as in Ref. [57]. The lattice parameters are identical to those in Ref. [48], except that for the tensor form factors the “residual matching factors” $\rho_{T\mu\nu}$ and the $\mathcal{O}(a)$ -improvement coefficients were set to their tree-level values, with appropriately increased estimates for the resulting systematic uncertainties as detailed further below. Following Ref. [48], two separate fits were performed to the lattice QCD data using BCL z -expansions [58] augmented with additional terms to describe the dependence on the lattice spacing and quark masses. The “nominal fit” is used to evaluate the central

f	J^P	m_{pole}^f (GeV)
h_+, h_\perp	1^-	6.332
$\tilde{h}_+, \tilde{h}_\perp$	1^+	6.768

Table 1. Values of the pole masses for the tensor form factors.

	Nominal fit	Higher-order fit
$a_0^{h_+}$	0.9752 ± 0.0303	0.9668 ± 0.0567
$a_1^{h_+}$	-5.5000 ± 1.2361	-4.5258 ± 1.7538
$a_2^{h_+}$		2.2006 ± 10.724
$a_0^{h_\perp}$	0.7054 ± 0.0137	0.7052 ± 0.0362
$a_1^{h_\perp}$	-4.3578 ± 0.5114	-4.1050 ± 0.8391
$a_2^{h_\perp}$		3.0100 ± 7.8351
$a_0^{\tilde{h}_+, \tilde{h}_+}$	0.6728 ± 0.0088	0.6763 ± 0.0328
$a_1^{\tilde{h}_+, \tilde{h}_+}$	-4.4322 ± 0.3882	-4.3634 ± 0.7509
$a_2^{\tilde{h}_+, \tilde{h}_+}$		2.2739 ± 8.0769
$a_1^{\tilde{h}_\perp, \tilde{h}_\perp}$	-4.4928 ± 0.3584	-4.5543 ± 0.7370
$a_2^{\tilde{h}_\perp, \tilde{h}_\perp}$		3.0851 ± 7.9037

Table 2. Results for the z -expansion parameters describing the $\Lambda_b \rightarrow \Lambda_c$ tensor form factors in the physical limit (in the $\overline{\text{MS}}$ scheme at the renormalization scale $\mu = m_b$). Files containing the values and covariances of the parameters of all ten $\Lambda_b \rightarrow \Lambda_c$ form factors are provided as supplemental material.

values and statistical uncertainties of the form factors (and of any observables depending on the form factors), while the “higher-order fit” is used in conjunction with the nominal fit to evaluate the combined systematic uncertainty associated with the continuum extrapolation, chiral extrapolation, z expansion, renormalization, scale setting, b -quark parameter tuning, finite volume, and missing isospin symmetry breaking/QED. The procedure for evaluating the systematic uncertainties is given in Eqs. (82)-(84) of Ref. [48]. The renormalization uncertainty in the tensor form factors is dominated by the use of the tree-level values, $\rho_{T^{\mu\nu}} = 1$, for the residual matching factors in the mostly nonperturbative renormalization procedure. We estimate the systematic uncertainty in $\rho_{T^{\mu\nu}}$ to be 2 times the maximum value of $|\rho_{V^\mu} - 1|$, $|\rho_{A^\mu} - 1|$, which is equal to 0.0404 [48]. Note that the tensor form factors are scale-dependent, and our results and estimates of systematic uncertainties should be interpreted as corresponding to $\mu = m_b$ in the $\overline{\text{MS}}$ scheme. To account for the renormalization uncertainty in the higher-order fit, we introduced nuisance parameters multiplying the form factors, with Gaussian priors equal to 1 ± 0.0404 .

In the physical limit (zero lattice spacing and physical quark masses), the nominal fit

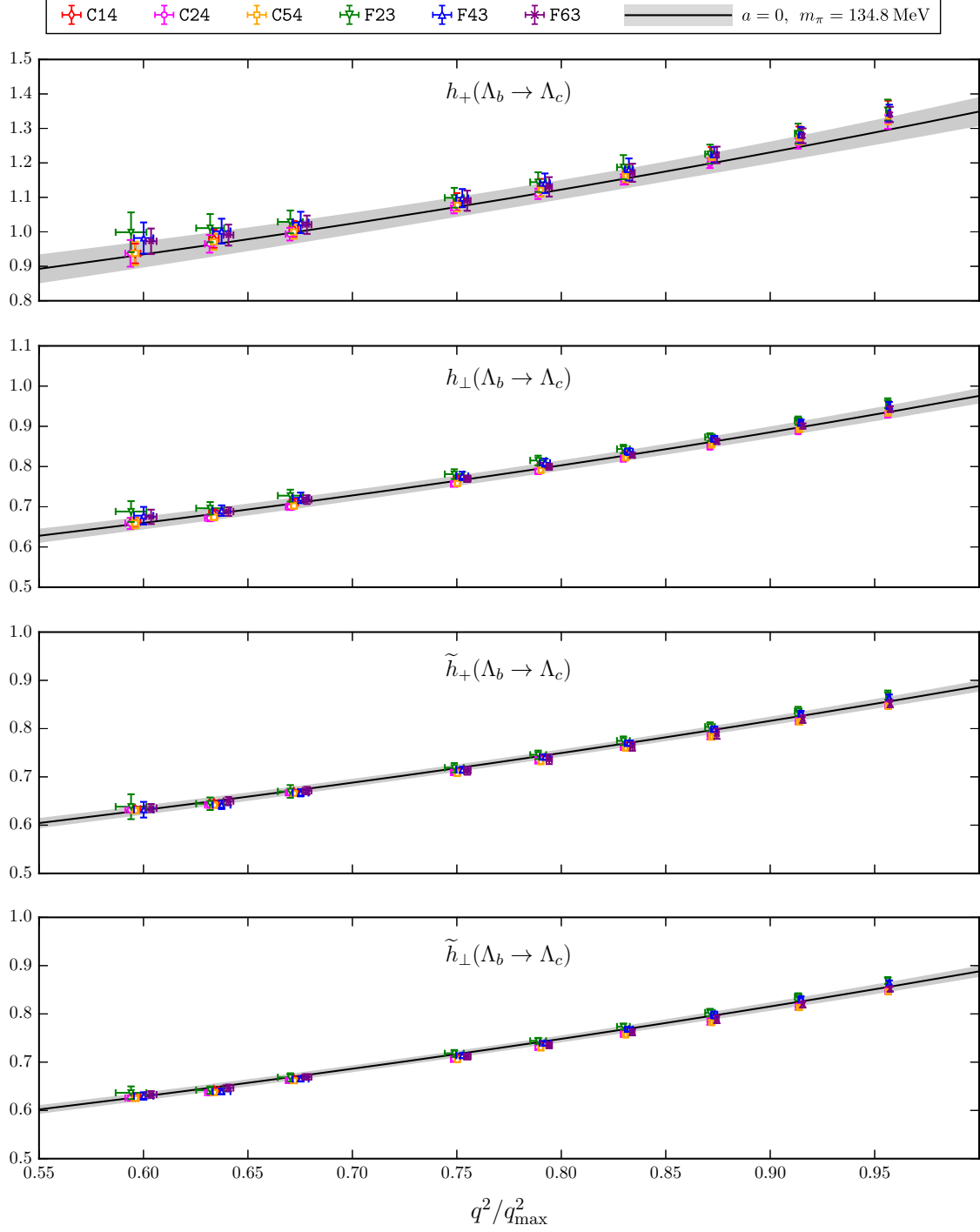


Figure 1. $\Lambda_b \rightarrow \Lambda_c$ tensor form factors in the high q^2 -region: lattice results and extrapolation to the physical limit (nominal fit). The bands indicate the statistical uncertainty. The lattice QCD data sets are labeled as in Ref. [48].

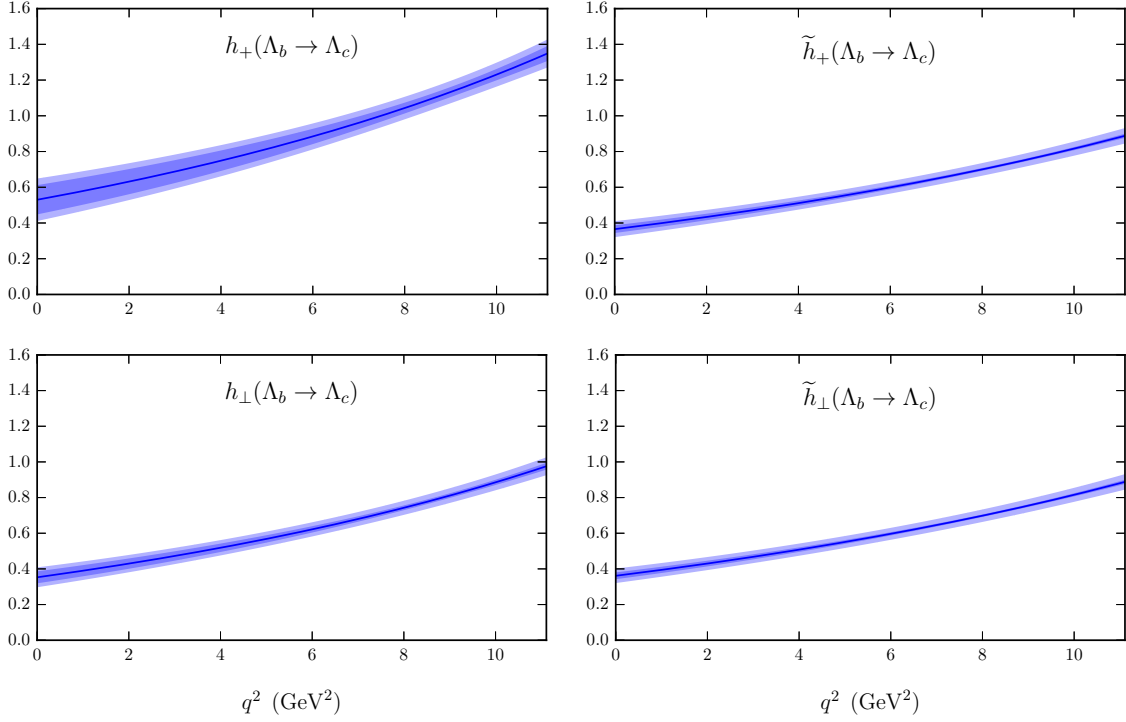


Figure 2. $\Lambda_b \rightarrow \Lambda_c$ tensor form factors in the physical limit, shown in the entire kinematic range. The form factors are defined in the $\overline{\text{MS}}$ scheme and at $\mu = m_b$. The inner bands show the statistical uncertainty and the outer bands show the total (statistical plus systematic) uncertainty. The procedure for evaluating the uncertainties using the nominal and higher-order fits is given in Eqs. (82)-(84) of Ref. [48].

function for a form factor f reduces to the form

$$f(q^2) = \frac{1}{1 - q^2/(m_{\text{pole}}^f)^2} [a_0^f + a_1^f z^f(q^2)], \quad (3.1)$$

while the higher-order fit function is given by

$$f_{\text{HO}}(q^2) = \frac{1}{1 - q^2/(m_{\text{pole}}^f)^2} [a_{0,\text{HO}}^f + a_{1,\text{HO}}^f z^f(q^2) + a_{2,\text{HO}}^f [z^f(q^2)]^2]. \quad (3.2)$$

The values of the pole masses are given in Table 1, and the kinematic variables z^f are defined as

$$z^f(q^2) = \frac{\sqrt{t_+^f - q^2} - \sqrt{t_+^f - t_0}}{\sqrt{t_+^f - q^2} + \sqrt{t_+^f - t_0}}, \quad (3.3)$$

$$t_0 = (m_{\Lambda_b} - m_{\Lambda_c})^2, \quad (3.4)$$

$$t_+^f = (m_{\text{pole}}^f)^2. \quad (3.5)$$

As in Ref. [48], in the fits to the lattice data we evaluated the pole masses as $am_{\text{pole}}^f = am_{B_c}^{(\text{lat})} + a\Delta^f$, where $am_{B_c}^{(\text{lat})}$ are the lattice QCD results for the pseudoscalar B_c mass on each individual data set, and the splittings Δ^f are fixed to their physical values $\Delta^{h_+, h_\perp} = 56$ MeV and $\Delta^{\tilde{h}_+, \tilde{h}_\perp} = 492$ MeV. The form factor results are very insensitive to the choices of Δ^f (as expected for poles far above q_{max}^2). When varying Δ^f by $\pm 10\%$, the z -expansion parameters returned from the fit are found to change in such a way that the changes in the form factors themselves are below 0.2% in the entire semileptonic region.

Plots of the lattice QCD data for the tensor form factors, along with the nominal fit functions in the physical limit, are shown in Fig. 1. The same fit functions are plotted in the entire kinematic range in Fig. 2, where also the total (statistical plus systematic) uncertainties are shown. The form factor h_+ has larger uncertainties than the other form factors because of larger excited-state contributions in the lattice QCD correlation functions.

The values of the nominal and higher-order fit parameters for the tensor form factors are given in Table 2. Because of the kinematic constraint

$$\tilde{h}_\perp(q_{\text{max}}^2) = \tilde{h}_+(q_{\text{max}}^2), \quad (3.6)$$

which is at the point $z = 0$, the form factors \tilde{h}_\perp and \tilde{h}_+ share the common parameters $a_0^{\tilde{h}_\perp, \tilde{h}_+}$. To evaluate the uncertainties of the form factors and of any observables depending on the form factors, it is essential to include the (cross-)correlations between all form factor parameters. The full covariance matrices of the nominal and higher-order parameters of all ten $\Lambda_b \rightarrow \Lambda_c$ form factors (vector, axial vector, and tensor) are provided as supplemental files.

4 Model-independent analysis of individual new-physics couplings

In this section we consider one new-physics coupling at a time. We first compute the constraints from the existing measurements with mesons, and then study the impact of a future measurement of $R(\Lambda_c)$.

4.1 Constraints from the existing measurements of $R(D)$, $R(D^*)$, and τ_{B_c}

We require the NP couplings to reproduce the measurements (1.7) and (1.8) of R_D^{Ratio} and $R_{D^*}^{\text{Ratio}}$ within the 3σ range. The coupling $g_S(g_P)$ only contributes to R_D^{Ratio} ($R_{D^*}^{\text{Ratio}}$) while the other couplings contribute to both channels. If only g_L is nonzero, the SM contribution gets rescaled by an overall factor $|1 + g_L|^2$, so that [31]

$$R_D^{\text{Ratio}} = R_{D^*}^{\text{Ratio}} = R_{\Lambda_c}^{\text{Ratio}} = |1 + g_L|^2, \quad (4.1)$$

which is consistent with the present measurements (1.7) and (1.8). Note that in the g_L -only scenario the forward-backward asymmetry (1.12) is unmodified, $A_{FB} = A_{FB}^{\text{SM}}$.

There is also a measurement of the τ polarization by Belle [59] with the result $P_\tau = -0.44 \pm 0.47_{-0.17}^{+0.20}$. The uncertainties of this measurement are presently too large to provide a significant additional constraint and we therefore do not include P_τ in our analysis.

	g_S only	g_P only	g_L only	g_R only	g_T only
	-0.4	0.3	-2.2	-0.044	0.4
$R(\Lambda_c)$	0.290 ± 0.009	0.342 ± 0.010	0.479 ± 0.014	0.344 ± 0.011	0.475 ± 0.037
$R_{\Lambda_c}^{Ratio}$	0.872 ± 0.007	1.026 ± 0.001	1.44	1.033 ± 0.003	1.426 ± 0.100
	$-1.5 - 0.3i$	$0.4 - 0.4i$	$0.15 - 0.3i$	$0.08 - 0.67i$	$0.2 - 0.2i$
$R(\Lambda_c)$	0.384 ± 0.013	0.346 ± 0.011	0.470 ± 0.014	0.465 ± 0.014	0.404 ± 0.021
$R_{\Lambda_c}^{Ratio}$	1.154 ± 0.008	1.040 ± 0.002	1.412	1.397 ± 0.005	1.213 ± 0.050

Table 3. The values of $R(\Lambda_c)$ and $R_{\Lambda_c}^{Ratio}$ for two example choices (real-valued and complex-valued) of the new-physics couplings. The standard-model value of $R(\Lambda_c)$ is 0.333 ± 0.010 [48]. The uncertainties given are due to the form factor uncertainties.

It was recently pointed out [47, 49, 50] that the measured lifetime of the B_c meson, $\tau_{B_c} = 0.507(9)$ ps [56], provides an upper bound on the $B_c \rightarrow \tau^- \bar{\nu}_\tau$ decay rate, which yields a strong constraint on the g_P coupling. According to SM calculations using an operator product expansion [60], only about 5% (for the central value) of the total width of the B_c , $\Gamma_{B_c} = 1/\tau_{B_c}$, can be attributed to purely tauonic and semi-tauonic modes. This can be relaxed as the parameters in the calculations are varied. In our analysis, we use an upper limit of $\mathcal{B}(B_c \rightarrow \tau^- \bar{\nu}_\tau) \leq 30\%$ to put constraints on the new-physics couplings. We use $f_{B_c} = 0.434(15)$ GeV from lattice QCD [61].

In Fig. 3, we present the constraints on the new-physics couplings coming from the measurements of R_D^{Ratio} , $R_{D^*}^{Ratio}$, and τ_{B_c} . We see that τ_{B_c} puts a strong constraint on g_P , and weak constraints on g_L and g_R . The tensor coupling g_T is strongly constrained by $R_{D^*}^{Ratio}$, and only weakly constrained by R_D^{Ratio} .

Example values of the ratios $R(\Lambda_c)$ and $R_{\Lambda_c}^{Ratio} = R(\Lambda_c)/R(\Lambda_c)^{SM}$ for representative allowed values of the NP couplings are given in Table 3. The standard-model prediction for $R(\Lambda_c)$ is 0.333 ± 0.010 [48]. We find that large deviations from this value are possible with the present mesonic constraints. In Table 4, we present the maximum and minimum allowed values of $R_{\Lambda_c}^{Ratio} = R(\Lambda_c)/R(\Lambda_c)^{SM}$ in the presence of each individual new-physics coupling, and the corresponding values of the coupling at which these occur.

Figure 4 shows the effect of representative values of the individual NP couplings on the $\Lambda_b \rightarrow \Lambda_c \tau \bar{\nu}_\tau$ differential decay rate (evaluated assuming $|V_{cb}| = 0.041$) as well as $B_{\Lambda_c}(q^2)$ [defined in Eq. (1.10)] and $A_{FB}(q^2)$. In all cases, except for the strongly constrained pure g_P coupling, substantial deviations from the SM predictions are allowed. We notice that A_{FB} is typically above the SM prediction in the presence of g_R or g_T , while it is typically below the SM prediction in the presence of g_S . Hence, it is possible to use A_{FB} to distinguish between the different couplings.

Coupling	$R(\Lambda_c)_{max}$	$R_{\Lambda_c, max}^{Ratio}$	coupling value	$R(\Lambda_c)_{min}$	$R_{\Lambda_c, min}^{Ratio}$	coupling value
g_S only	0.405	1.217	0.363	0.314	0.942	-1.14
g_P only	0.354	1.062	0.658	0.337	1.014	0.168
g_L only	0.495	1.486	$0.094 + 0.538i$	0.340	1.022	$-0.070 + 0.395i$
g_R only	0.525	1.576	$0.085 + 0.793i$	0.336	1.009	-0.012
g_T only	0.526	1.581	0.428	0.338	1.015	-0.005

Table 4. The maximum and minimum values of $R(\Lambda_c)$ and $R_{\Lambda_c}^{Ratio}$ allowed by the mesonic constraints for each new-physics coupling, and the coupling values at which these extrema are reached.

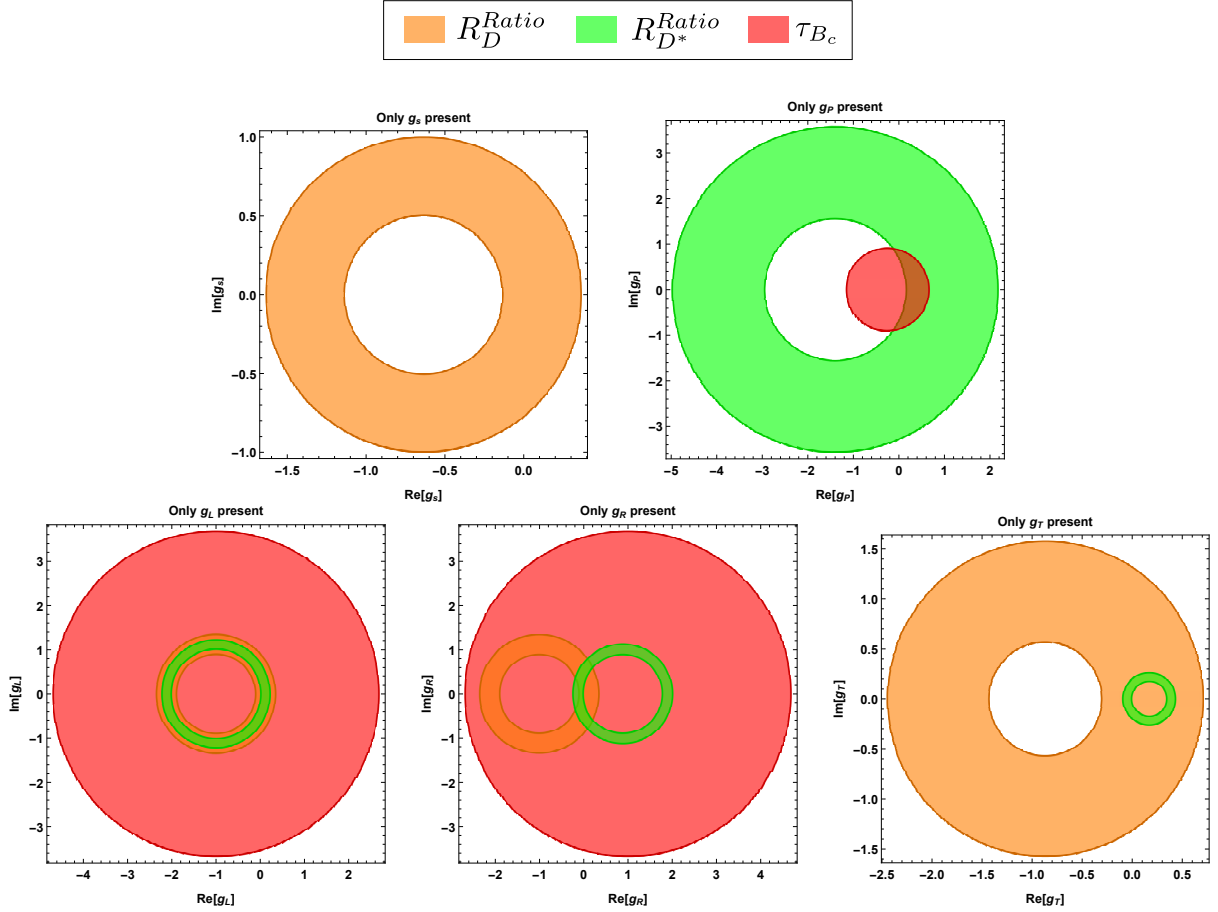


Figure 3. Constraints on the individual new-physics couplings from the measurements of R_D^{Ratio} , $R_{D^*}^{Ratio}$, and τ_{B_c} . We require that the couplings reproduce the measurements of R_D^{Ratio} and $R_{D^*}^{Ratio}$ in Eqs. (1.7) and (1.8) within 3σ , and satisfy $\mathcal{B}(B_c \rightarrow \tau^- \bar{\nu}_\tau) \leq 30\%$.

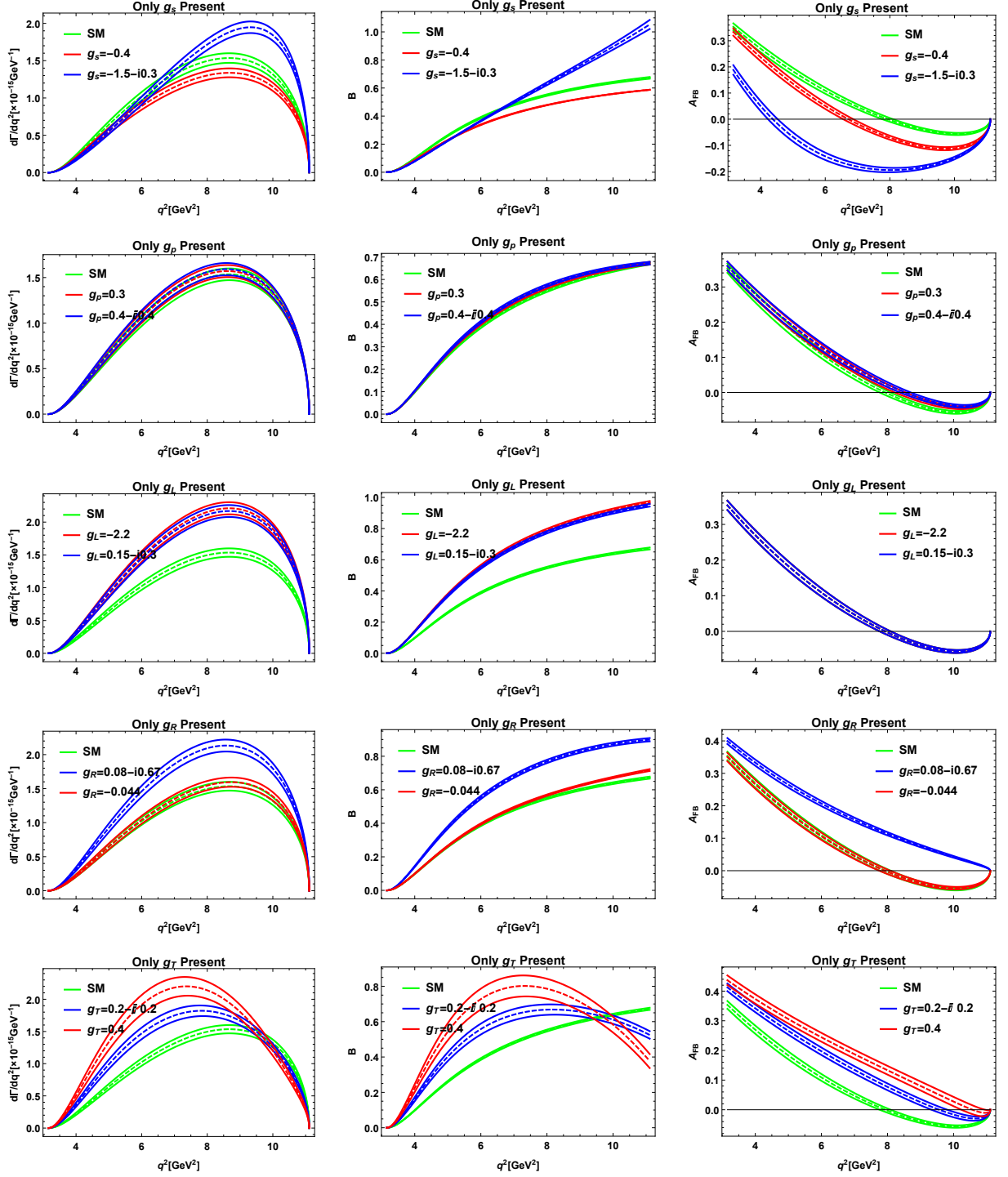


Figure 4. The effect of individual new-physics couplings on the $\Lambda_b \rightarrow \Lambda_c \tau \bar{\nu}_\tau$ differential decay rate (left), the ratio of the $\Lambda_b \rightarrow \Lambda_c \tau \bar{\nu}_\tau$ and $\Lambda_b \rightarrow \Lambda_c \ell \bar{\nu}_\ell$ differential decay rates (middle), and the $\Lambda_b \rightarrow \Lambda_c \tau \bar{\nu}_\tau$ forward-backward asymmetry (right). Each plot shows the observable in the Standard Model and for two representative values of the new-physics coupling (one real-valued choice and one complex-valued choice). The bands indicate the 1σ uncertainties originating from the $\Lambda_b \rightarrow \Lambda_c$ form factors.

4.2 Impact of a future $R(\Lambda_c)$ measurement

In this subsection we present the effect of possible future measurements of $R(\Lambda_c)$ on the NP couplings constraints. We consider two cases, one in which the measured value is near the SM prediction and one with measured value far from SM. For the first case we take $R_{\Lambda_c}^{Ratio} = 1 \pm 3 \times 0.05$, and for the second case $R_{\Lambda_c}^{Ratio} = 1.3 \pm 3 \times 0.05$ (the same central values as R_D^{Ratio}). Note that we take the 1σ uncertainty as 0.05. Figures 5 and 6 show the allowed regions of the parameter space for the first and second case, respectively. We observe the following when adding the $R_{\Lambda_c}^{Ratio}$ constraints to the mesonic constraints:

- For $R(\Lambda_c)$ near the SM (Fig. 5), the allowed regions for (g_L, g_R, g_T) are reduced significantly, the allowed region for g_S shrinks only slightly, and the allowed region for g_P remains the same (as it is dominantly constrained by τ_{B_c}).
- For $R(\Lambda_c)$ far from the SM (Fig. 6), most of the previously allowed region for g_S becomes excluded by $R(\Lambda_c)$. Even more importantly, the g_P -only scenario becomes ruled out. In this case, $R(\Lambda_c)$ also provides strong constraints on (g_L, g_R, g_T) , but these constraints still overlap with the mesonic constraints.

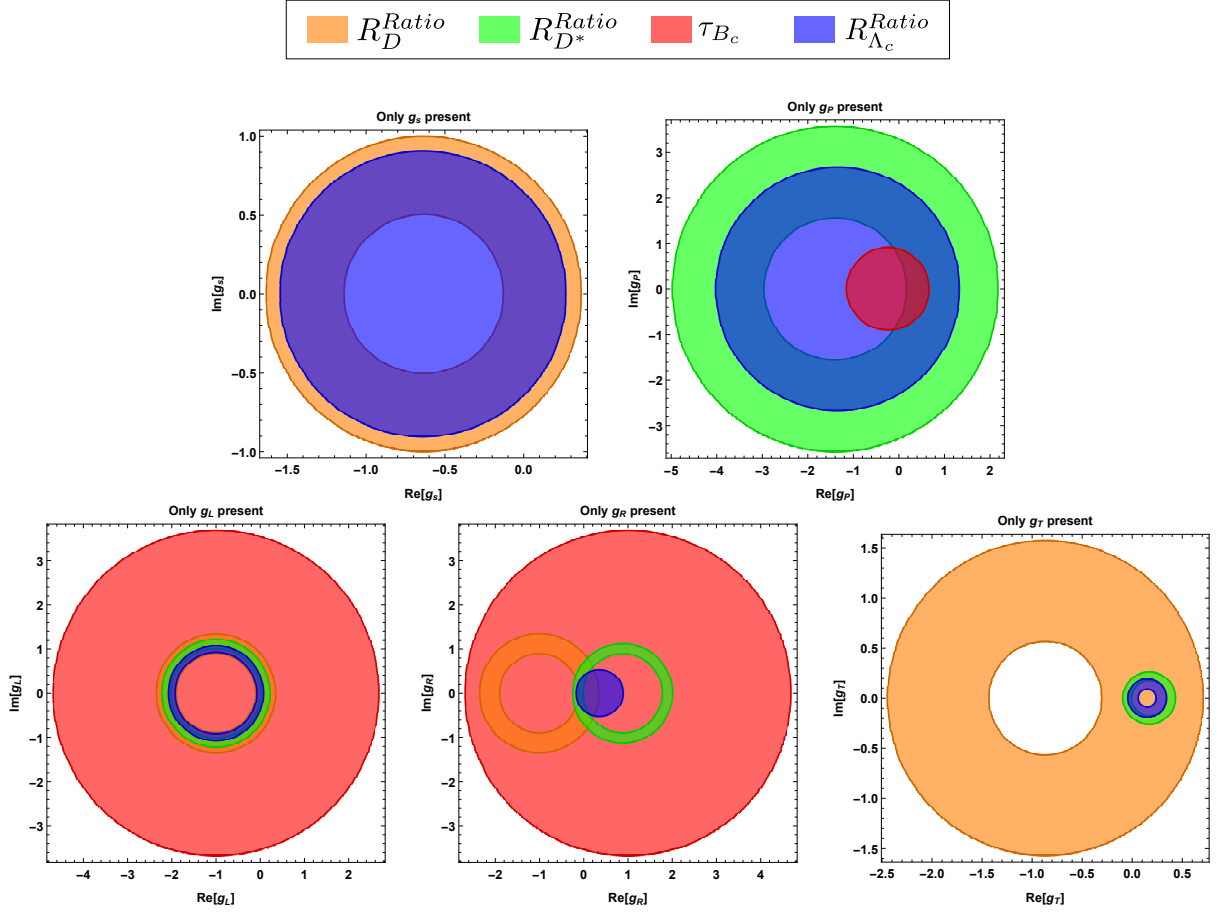


Figure 5. Constraints on individual new-physics couplings from a possible $R(\Lambda_c)$ measurement (shown in blue), assuming that $R_{\Lambda_c}^{Ratio} = 1 \pm 3 \times 0.05$ where the 1σ uncertainty is 0.05. Also shown are the mesonic constraints as in Fig. 3.

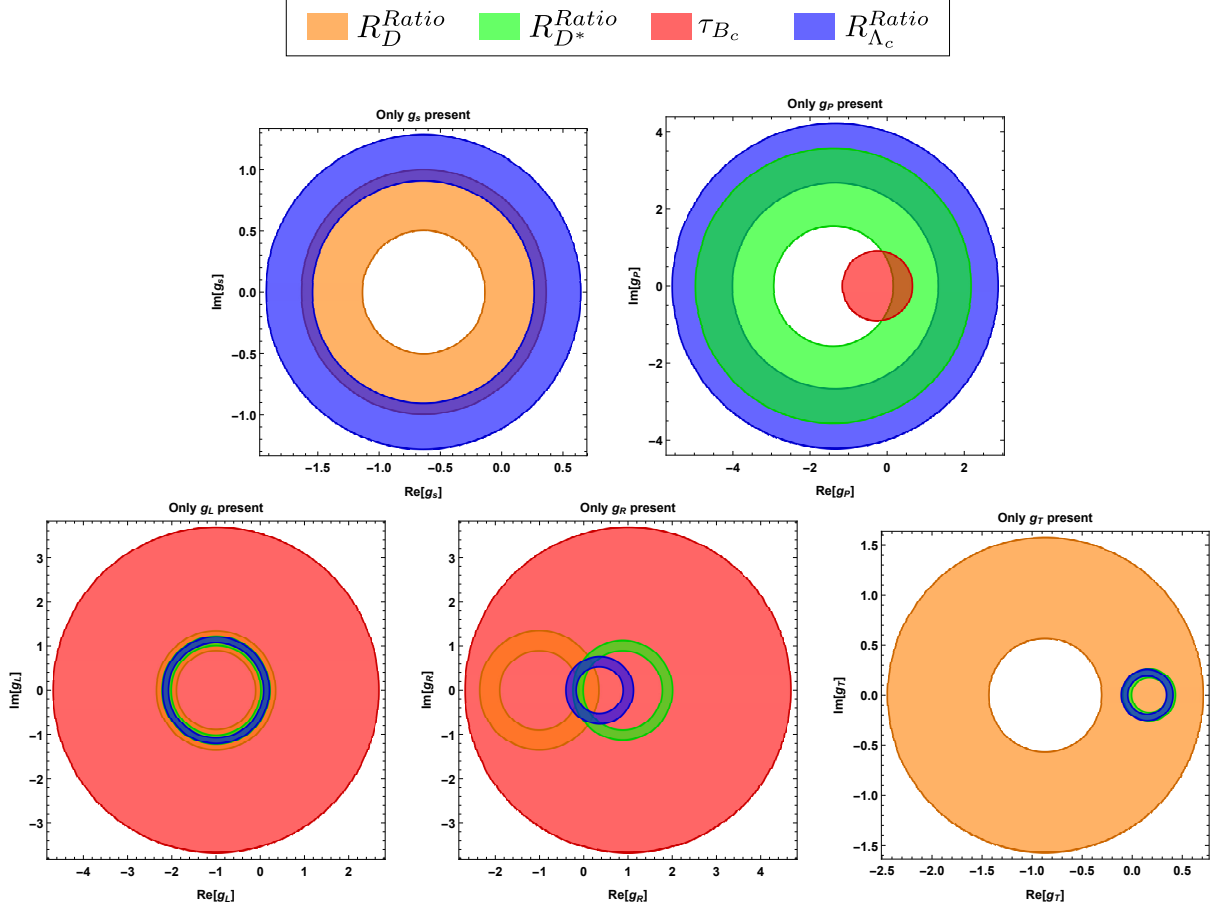


Figure 6. Constraints on individual new-physics couplings from a possible $R(\Lambda_c)$ measurement (shown in blue), assuming that $R_{\Lambda_c}^{Ratio} = 1.3 \pm 3 \times 0.05$ where the 1σ uncertainty is 0.05. Also shown are the mesonic constraints as in Fig. 3.

5 Explicit models

In this section we will discuss explicit models that can generate the couplings in the effective Hamiltonian (2.1). We will consider three categories: Two-Higgs-doublet models which generate (g_S, g_P) , $SU(2)$ models which generate g_L , and leptoquark models which generate (g_S, g_P, g_L, g_T) . We do not consider models that generate g_R , as in the standard-model-effective-theory picture it is difficult to have a g_R coupling that leads to lepton universality violation effects [62].

5.1 Two-Higgs-doublet models

The simplest scalar extensions of the SM are the two-Higgs-doublet models (2HDM). The 2HDM of type II is disfavored by experiment [1]. We will consider the Aligned Two-Higgs-Doublet Model (A2HDM) from Ref. [21]. The Lagrangian of the model is

$$\mathcal{L}_Y^{H^\pm} = -\frac{\sqrt{2}}{v} H^+ \{ \bar{u} [\xi_d V M_d \mathcal{P}_R - \xi_u M_u V \mathcal{P}_L] d + \xi_l \bar{\nu} M_l \mathcal{P}_R l \} + \text{h.c.}, \quad (5.1)$$

where u , d , and l denote all three generations of up-type quarks, down-type quarks, and charged leptons, M_u and M_d are the quark mass matrices, and V is the CKM matrix. Above, ξ_f ($f = u, d, l$) are the proportionality parameters in the so-called ‘‘Higgs basis’’, in which only one scalar doublet acquires a nonzero vacuum expectation value. The cases $\xi_d = \xi_l = -1/\xi_u = -\tan \beta$ and $\xi_u = \xi_d = \xi_l = \cot \beta$ correspond to the Type-II and Type-I models, respectively. The general effective couplings in Eq. (2.1) read

$$\begin{aligned} g_S^{quqd} &= g_R^{quqd} + g_L^{quqd}, \\ g_P^{quqd} &= g_R^{quqd} - g_L^{quqd}, \end{aligned} \quad (5.2)$$

where

$$g_L^{quqd} = \xi_u \xi_l^* \frac{m_{q_u} m_l}{M_{H^\pm}^2}, \quad g_R^{quqd} = -\xi_d \xi_l^* \frac{m_{q_d} m_l}{M_{H^\pm}^2}. \quad (5.3)$$

The scenario in which the $\xi_{u,d,l}$ parameters are universal for all three generations is ruled out [21]. We therefore assume that Eq. (5.3) only gives the couplings for processes involving the b quark, while the couplings for the first two generations are considered independently. In this model we find significant deviation from the standard model contribution to the decay $\Lambda_b \rightarrow \Lambda_c \tau \bar{\nu}_\tau$, but for a more complete analysis RGE evolution should be considered. The RGE evolution of the couplings of the A2HDM has been discussed in Ref. [63]. The alignment condition, which guarantees the absence of tree-level FCNC processes, is preserved by the RGE only in the case of the standard type-I, II, X, and Y models which are discussed in [64]. However, our framework requires non-universal flavor dependent couplings and the RGE evolution has not been worked out and is not included in the analysis. Keeping in mind that RGE effects could change the phenomenology of the model, the discussion of the full numerical analysis of the model is not included in this work.

5.2 $SU(2)$ and Leptoquark models

The analysis of the $R(D^{(*)})$ and R_K anomalies could favor the left-handed operator g_L . In Ref. [31], it was pointed out that, assuming that the scale of NP is much higher than the weak scale, the g_L operator should be invariant under the full $SU(3)_C \times SU(2)_L \times U(1)_Y$ gauge group. There are two possibilities:

$$\begin{aligned}\mathcal{O}_1^{NP} &= \frac{G_1}{\Lambda_{\text{NP}}^2} (\bar{Q}'_L \gamma_\mu Q'_L) (\bar{L}'_L \gamma^\mu L'_L) , \\ \mathcal{O}_2^{NP} &= \frac{G_2}{\Lambda_{\text{NP}}^2} (\bar{Q}'_L \gamma_\mu \sigma^I Q'_L) (\bar{L}'_L \gamma^\mu \sigma^I L'_L) \\ &= \frac{G_2}{\Lambda_{\text{NP}}^2} \left[2(\bar{Q}'_L \gamma_\mu Q'^j_L) (\bar{L}'_L \gamma^\mu L'^j_L) - (\bar{Q}'_L \gamma_\mu Q'_L) (\bar{L}'_L \gamma^\mu L'_L) \right] ,\end{aligned}\quad (5.4)$$

where G_1 and G_2 are both $O(1)$, and the σ^I are the Pauli matrices. Here $Q' \equiv (t', b')^T$ and $L' \equiv (\nu'_\tau, \tau')^T$. The key point is that \mathcal{O}_2^{NP} contains both neutral-current (NC) and charged-current (CC) interactions. The NC and CC pieces can be used to respectively explain the R_K and $R(D^{(*)})$ puzzles. In the following, we briefly review the literature on models of this type.

In Ref. [36], UV completions that can give rise to $\mathcal{O}_{1,2}^{NP}$ [Eq. (5.4)], were discussed. One among the four possibilities for the underlying NP model is a vector boson (VB) that transforms as $(\mathbf{1}, \mathbf{3}, 0)$ under $SU(3)_C \times SU(2)_L \times U(1)_Y$, as in the SM.

Concrete VB models were discussed in Ref. [37, 38] and the simplest VB model was considered in Ref. [39]. We refer to the VBs as $V = W', Z'$. In the gauge basis, the Lagrangian describing the couplings of the VBs to left-handed third-generation fermions is

$$\Delta\mathcal{L}_V = g_{qV}^{33} \left(\bar{Q}'_{L3} \gamma^\mu \sigma^I Q'_{L3} \right) V_\mu^I + g_{\ell V}^{33} \left(\bar{L}'_{L3} \gamma^\mu \sigma^I L'_{L3} \right) V_\mu^I , \quad (5.5)$$

where σ^I ($I = 1, 2, 3$) are the Pauli matrices. Once the heavy VB is integrated out, one obtains the following effective Lagrangian, relevant for $b \rightarrow s\ell^+\ell^-$, $b \rightarrow c\tau^-\bar{\nu}$ and $b \rightarrow s\nu\bar{\nu}$ decays:

$$\mathcal{L}_V^{\text{eff}} = -\frac{g_{qV}^{33} g_{\ell V}^{33}}{m_V^2} \left(\bar{Q}'_{L3} \gamma^\mu \sigma^I Q'_{L3} \right) \left(\bar{L}'_{L3} \gamma_\mu \sigma^I L'_{L3} \right) . \quad (5.6)$$

One can study the phenomenology of the model with an ansatz for the mixing matrices. The assumption of Ref. [36, 39] is that the transformations D and L involve only the second and third generations. The key observation in Ref. [39] is the Z' interaction also contributes to B_s mixing and the model becomes highly constrained. In fact only a few percent deviation from the SM is allowed in the $R(D^{(*)})$ observables. For this reason, we do not present a detailed numerical analysis of the $SU(2)$ models for the $\Lambda_b \rightarrow \Lambda_c \tau \bar{\nu}_\tau$ decay.

We next move to leptoquark models. In Ref. [65], several leptoquark models are considered that generate scalar, vector, and tensor operators. The $SU(3) \times SU(2) \times U(1)$ quantum numbers of these models are summarized in Table 5. We can group the leptoquarks as vector or scalar leptoquarks. These leptoquarks can in turn be $SU(2)$ singlets, doublets, or triplets.

	spin	$SU(3)_c$	$SU(2)_L$	$U(1)_{Y=Q-T_3}$
S_1	0	3^*	1	1/3
\mathbf{S}_3	0	3^*	3	1/3
R_2	0	3	2	7/6
V_2	1	3^*	2	5/6
U_1	1	3	1	2/3
\mathbf{U}_3	1	3	3	2/3

Table 5. Quantum numbers of scalar and vector leptoquarks.

The Lagrangians for the various leptoquarks are

$$\mathcal{L}^{\text{LQ}} = \mathcal{L}_V^{\text{LQ}} + \mathcal{L}_S^{\text{LQ}}, \quad (5.7)$$

$$\begin{aligned} \mathcal{L}_V^{\text{LQ}} = & \left(h_{1L}^{ij} \bar{Q}_L^i \gamma_\mu L_L^j + h_{1R}^{ij} \bar{d}_R^i \gamma_\mu \ell_R^j \right) U_1^\mu + h_{3L}^{ij} \bar{Q}_L^i \boldsymbol{\sigma} \gamma_\mu L_L^j \mathbf{U}_3^\mu \\ & + \left(g_{2L}^{ij} \bar{d}_R^{c,i} \gamma_\mu L_L^j + g_{2R}^{ij} \bar{Q}_L^{c,i} \gamma_\mu \ell_R^j \right) V_2^\mu + \text{h.c.} \end{aligned} \quad (5.8)$$

$$\begin{aligned} \mathcal{L}_S^{\text{LQ}} = & \left(g_{1L}^{ij} \bar{Q}_L^{c,j} i \sigma_2 L_L^j + g_{1R}^{ij} \bar{u}_R^{c,i} \ell_R^j \right) S_1 + g_{3L}^{ij} \bar{Q}_L^{c,i} i \sigma_2 \boldsymbol{\sigma} L_L^j \mathbf{S}_3 \\ & + \left(h_{2L}^{ij} \bar{u}_R^i L_L^j + h_{2R}^{ij} \bar{Q}_L^i i \sigma_2 \ell_R^j \right) R_2 + \text{h.c.}, \end{aligned} \quad (5.9)$$

where h^{ij} and g^{ij} are dimensionless couplings, S_1 , \mathbf{S}_3 , and R_2 are the scalar leptoquark bosons, U_1^μ , \mathbf{U}_3^μ , and V_2^μ are the vector leptoquark bosons, and the index i (j) indicates the generation of quarks (leptons).

The leptoquark Lagrangian generates the following couplings in Eq. (2.1):

$$g_S(\mu_b) = \frac{\sqrt{2}}{4G_F V_{cb}} (C_{S_1}(\mu_b) + C_{S_2}(\mu_b)), \quad (5.10)$$

$$g_P(\mu_b) = \frac{\sqrt{2}}{4G_F V_{cb}} (C_{S_1}(\mu_b) - C_{S_2}(\mu_b)), \quad (5.11)$$

$$g_L = \frac{\sqrt{2}}{4G_F V_{cb}} C_{\mathcal{V}_1}^l, \quad (5.12)$$

$$g_R = \frac{\sqrt{2}}{4G_F V_{cb}} C_{\mathcal{V}_2}^l, \quad (5.13)$$

$$g_T(\mu_b) = \frac{\sqrt{2}}{4G_F V_{cb}} C_{\mathcal{T}}(\mu_b), \quad (5.14)$$

where the Wilson coefficients in the leptoquark models are given by

$$C_{\text{SM}} = 2\sqrt{2}G_F V_{cb}, \quad (5.15)$$

$$C_{\mathcal{V}_1}^l = \sum_{k=1}^3 V_{k3} \left[\frac{g_{1L}^{kl} g_{1L}^{23*}}{2M_{S_1}^2} - \frac{g_{3L}^{kl} g_{3L}^{23*}}{2M_{S_3}^2} + \frac{h_{1L}^{2l} h_{1L}^{k3*}}{M_{U_1}^2} - \frac{h_{3L}^{2l} h_{3L}^{k3*}}{M_{U_3}^2} \right], \quad (5.16)$$

$$C_{\mathcal{V}_2}^l = 0, \quad (5.17)$$

$$C_{S_1}^l = \sum_{k=1}^3 V_{k3} \left[-\frac{2g_{2L}^{kl} g_{2R}^{23*}}{M_{V_2}^2} - \frac{2h_{1L}^{2l} h_{1R}^{k3*}}{M_{U_1}^2} \right], \quad (5.18)$$

$$C_{S_2}^l = \sum_{k=1}^3 V_{k3} \left[-\frac{g_{1L}^{kl} g_{1R}^{23*}}{2M_{S_1}^2} - \frac{h_{2L}^{2l} h_{2R}^{k3*}}{2M_{R_2}^2} \right], \quad (5.19)$$

$$C_{\mathcal{T}}^l = \sum_{k=1}^3 V_{k3} \left[\frac{g_{1L}^{kl} g_{1R}^{23*}}{8M_{S_1}^2} - \frac{h_{2L}^{2l} h_{2R}^{k3*}}{8M_{R_2}^2} \right]. \quad (5.20)$$

These Wilson coefficients are defined at the energy scale $\mu = M_X$, where X represents a leptoquark. Above, V_{k3} denotes the relevant CKM matrix element, where the 3 corresponds to the bottom quark. In the following, we neglect the CKM-suppressed contributions from $k = 1$ and $k = 2$ in the sums. Because the neutrino is not observed, we have $l = 1, 2, 3$. Note that there is a Standard-Model contribution for $l = 3$ but not for $l = 1, 2$; hence, the constraints for different l will be different.

The renormalization-group running of the scalar and tensor Wilson coefficients from $\mu = M_X$ to $\mu = \mu_b$, where μ_b is the mass scale of the bottom quark, is given by

$$C_{S_{1,2}}(\mu_b) = \left[\frac{\alpha_s(m_t)}{\alpha_s(\mu_b)} \right]^{-\frac{12}{23}} \left[\frac{\alpha_s(m_{\text{LQ}})}{\alpha_s(m_t)} \right]^{-\frac{4}{7}} C_{S_{1,2}}(m_{\text{LQ}}), \quad (5.21)$$

$$C_{\mathcal{T}}(\mu_b) = \left[\frac{\alpha_s(m_t)}{\alpha_s(\mu_b)} \right]^{\frac{4}{23}} \left[\frac{\alpha_s(m_{\text{LQ}})}{\alpha_s(m_t)} \right]^{\frac{4}{21}} C_{\mathcal{T}}(m_{\text{LQ}}), \quad (5.22)$$

where $\alpha_s(\mu)$ is the QCD coupling at scale μ . Because the anomalous dimensions of the vector and axial-vector currents are zero, the Wilson coefficients for $\mathcal{V}_{1,2}$ are scale-independent.

The different leptoquarks produce different effective operators as summarized below:

- The S_1 leptoquark with nonzero (g_{1L}, g_{1R}^*) generates $C_{\mathcal{V}_1}^l$, $C_{S_2}^l$, and $C_{\mathcal{T}}^l$, with the relation $C_{S_2}^l = -4C_{\mathcal{T}}^l$.
- The R_2 leptoquark with (h_{2L}, h_{2R}^*) generates $C_{S_2}^l$ and $C_{\mathcal{T}}^l$ with the relation $C_{S_2}^l = 4C_{\mathcal{T}}^l$.
- The V_2 leptoquark generates $C_{S_1}^l$ and is tightly constrained, so we do not consider this model.
- The U_1 leptoquark with nonzero (g_{2L}, g_{2R}^*) generates $C_{S_1}^l$ and $C_{\mathcal{V}_1}^l$.
- The S_3 and U_3 leptoquarks with nonzero values of (g_{3L}, g_{3L}^*) and (h_{3L}, h_{3L}^*) generate $C_{\mathcal{V}_1}^l$.

The leptoquark couplings can also be constrained using $b \rightarrow s\nu\bar{\nu}$ decays. As pointed out in Ref. [39], the exclusive decays $\bar{B} \rightarrow K\nu\bar{\nu}$ and $\bar{B} \rightarrow K^*\nu\bar{\nu}$ provide more stringent bounds than the inclusive mode $B \rightarrow X_s\nu\bar{\nu}$. The U_1 and R_2 leptoquarks do not contribute to $b \rightarrow s\nu\bar{\nu}$, while the left-handed couplings of S_1 , S_3 , and U_3 do. (The V_2 leptoquark also contributes to $b \rightarrow s\nu\bar{\nu}$, but we do not consider this model.) The BaBar and Belle Collaborations give the following 90% C.L. upper limits [66, 67]:

$$\begin{aligned}\mathcal{B}(B^+ \rightarrow K^+\nu\bar{\nu}) &\leq 1.7 \times 10^{-5}, \\ \mathcal{B}(B^+ \rightarrow K^{*+}\nu\bar{\nu}) &\leq 4.0 \times 10^{-5}, \\ \mathcal{B}(B^0 \rightarrow K^{*0}\nu\bar{\nu}) &\leq 5.5 \times 10^{-5}.\end{aligned}\tag{5.23}$$

In Ref. [68], these are compared with the SM predictions

$$\begin{aligned}\mathcal{B}_K^{\text{SM}} &\equiv \mathcal{B}(B \rightarrow K\nu\bar{\nu})_{\text{SM}} = (3.98 \pm 0.43 \pm 0.19) \times 10^{-6}, \\ \mathcal{B}_{K^*}^{\text{SM}} &\equiv \mathcal{B}(B \rightarrow K^*\nu\bar{\nu})_{\text{SM}} = (9.19 \pm 0.86 \pm 0.50) \times 10^{-6}.\end{aligned}\tag{5.24}$$

Taking into account the theoretical uncertainties [68], the 90% C.L. upper bounds on the NP contributions are

$$\frac{\mathcal{B}_K^{\text{SM+NP}}}{\mathcal{B}_K^{\text{SM}}} \leq 4.8, \quad \frac{\mathcal{B}_{K^*}^{\text{SM+NP}}}{\mathcal{B}_{K^*}^{\text{SM}}} \leq 4.9.\tag{5.25}$$

Following Ref. [8], the $b \rightarrow s\nu_j\bar{\nu}_i$ process can be described by the effective Hamiltonian

$$H_{eff} = \frac{4G_F}{\sqrt{2}} V_{tb} V_{ts}^* \left[\left(\delta_{ij} C_L^{(\text{SM})} + C_L^{ij} \right) O_L^{ij} + C_R^{ij} O_R^{ij} \right],\tag{5.26}$$

where the left-handed and right-handed operators are defined as

$$\begin{aligned}O_L^{ij} &= (\bar{s}_L \gamma^\mu b_L) (\bar{\nu}_{jL} \gamma_\mu \nu_{iL}), \\ O_R^{ij} &= (\bar{s}_R \gamma^\mu b_R) (\bar{\nu}_{jL} \gamma_\mu \nu_{iL}).\end{aligned}\tag{5.27}$$

The SM Wilson coefficient $C_L^{(\text{SM})}$ receives contributions from box and Z -penguin diagrams, which yield

$$C_L^{(\text{SM})} = \frac{\alpha}{2\pi \sin^2 \theta_W} X(m_t^2/M_W^2),\tag{5.28}$$

where the loop function $X(x_t)$ can be found e.g. in Ref. [69]. The leptoquarks that we consider produce contributions to C_L^{ij} which, to leading order, are equal to [8]

$$C_L^{ij} = -\frac{1}{2\sqrt{2}G_F V_{tb} V_{ts}^*} \left[\frac{g_{1L}^{3i} g_{1L}^{2j*}}{2M_{S_1}^2} + \frac{g_{3L}^{3i} g_{3L}^{2j*}}{2M_{S_3}^2} - \frac{2h_{3L}^{2i} h_{3L}^{3j*}}{M_{U_3}^2} \right].\tag{5.29a}$$

We obtain common coefficients for $b \rightarrow c\tau\bar{\nu}_l$ and $b \rightarrow s\nu_\tau\bar{\nu}_l$ processes,

$$C_L^{l3} = -\frac{1}{2\sqrt{2}G_F V_{tb} V_{ts}^*} \left[\frac{g_{1L}^{3l} g_{1L}^{23*}}{2M_{S_1}^2} + \frac{g_{3L}^{3l} g_{3L}^{23*}}{2M_{S_3}^2} - \frac{2h_{3L}^{2l} h_{3L}^{33*}}{M_{U_3}^2} \right]. \quad (5.30a)$$

Hence, for $l = 3$ we obtain

$$\frac{\mathcal{B}_K^{\text{SM+NP}}}{\mathcal{B}_K^{\text{SM}}} = \frac{\mathcal{B}_{K^*}^{\text{SM+NP}}}{\mathcal{B}_{K^*}^{\text{SM}}} = \left| \frac{3C_L^{(\text{SM})} + C_L^{33}}{3C_L^{(\text{SM})}} \right|^2, \quad (5.31)$$

while for $l = 1, 2$ we have

$$\frac{\mathcal{B}_K^{\text{SM+NP}}}{\mathcal{B}_K^{\text{SM}}} = \frac{\mathcal{B}_{K^*}^{\text{SM+NP}}}{\mathcal{B}_{K^*}^{\text{SM}}} = \left| \frac{C_L^{l3}}{3C_L^{(\text{SM})}} \right|^2. \quad (5.32)$$

When considering nonzero values only for one coupling at a time ($l = 1, 2, 3$), the experimental measurements of R_D^{Ratio} , $R_{D^*}^{\text{Ratio}}$, τ_{B_c} , and $\mathcal{B}(B \rightarrow K^{(*)}\nu\bar{\nu})$ yield the constraints shown in Figures 7, 8, and 9. The cases with $g_{3L}^{3i} g_{3L}^{23*}$ in the \mathbf{S}_3 model, $g_{1L}^{3i} g_{1L}^{23*}$ in the \mathbf{S}_1 model, and $h_{3L}^{2i} h_{3L}^{23*}$ in the \mathbf{U}_3 model are ruled out for $i = 1, 2$.

Allowing all relevant couplings in each model to be nonzero simultaneously, we obtain the coupling regions sampled by the random points in Figs. 10 and 11. The corresponding allowed regions in the $R_{\Lambda_c}^{\text{Ratio}} - R_D^{\text{Ratio}}$ and $R_{\Lambda_c}^{\text{Ratio}} - R_{D^*}^{\text{Ratio}}$ planes are shown in Fig. 12. Since the \mathbf{S}_3 and \mathbf{U}_3 leptoquarks produce only the vector coupling g_L , all ratios get rescaled by the common factor of $|1 + g_L|^2$. The \mathbf{S}_3 and \mathbf{U}_3 models are tightly constrained and only small effects are allowed. The other leptoquark models can produce substantial effects in $R_{\Lambda_c}^{\text{Ratio}}$, with varying degrees of correlation between the mesonic and baryonic observables.

The values of $R(\Lambda_c)$ and $R_{\Lambda_c}^{\text{Ratio}}$ for two typical allowed combinations of the couplings in each model are given in Table 6. In Fig. 13, we present plots of the observables ($d\Gamma/dq^2$, B_{Λ_c} , A_{FB}) for the same values of the couplings.

Model	Case	Couplings	$R(\Lambda_c)$	$R_{\Lambda_c}^{Ratio}$
S_1	1	$g_{1L}^{33} g_{1R}^{23*} = 0.332 + 0.403i,$ $g_{1L}^{3i} g_{1R}^{23*} = 0.417 - 0.311i,$ $g_{1L}^{33} g_{1L}^{23*} = 0.015 - 0.037i,$ $g_{1L}^{3i} g_{1L}^{23*} = -0.079 - 0.002i$	0.343 ± 0.011	1.032 ± 0.004
S_1	2	$g_{1L}^{33} g_{1R}^{23*} = 0.064 - 0.142i,$ $g_{1L}^{3i} g_{1R}^{23*} = -1.05 + 0.638i,$ $g_{1L}^{33} g_{1L}^{23*} = 0.116 - 0.043i,$ $g_{1L}^{3i} g_{1L}^{23*} = 0.018 + 0.104i$	0.549 ± 0.020	1.648 ± 0.025
R_2	1	$h_{2L}^{23} h_{2R}^{33*} = 0.373 - 0.118i,$ $h_{2L}^{2i} h_{2R}^{33*} = -0.846 - 0.191i$	0.445 ± 0.016	1.337 ± 0.016
R_2	2	$h_{2L}^{23} h_{2R}^{33*} = 0.753 - 0.199i,$ $h_{2L}^{2i} h_{2R}^{33*} = 0.897 - 0.031i$	0.485 ± 0.018	1.455 ± 0.025
U_1	1	$h_{1L}^{23} h_{1R}^{33*} = -0.115 - 0.021i,$ $h_{1L}^{2i} h_{1R}^{33*} = 0.049 + 0.159i,$ $h_{1L}^{23} h_{1L}^{33*} = -1.468 + 0.271i,$ $h_{1L}^{2i} h_{1L}^{33*} = 1.116 + 0.744i$	0.605 ± 0.019	1.818 ± 0.008
U_1	2	$h_{1L}^{23} h_{1R}^{33*} = -0.059 + 0.236i,$ $h_{1L}^{2i} h_{1R}^{33*} = 0.234 + 0.105i,$ $h_{1L}^{23} h_{1L}^{33*} = -2.002 + 0.854i,$ $h_{1L}^{2i} h_{1L}^{33*} = -0.135 + 0.940i$	0.553 ± 0.018	1.663 ± 0.005
S_3	1	$g_{3L}^{33} g_{3L}^{23*} = -0.035 + 0.032i,$ $g_{3L}^{3i} g_{3L}^{23*} = 0.061 + 0.041i$	0.342 ± 0.010	1.027
S_3	2	$g_{3L}^{33} g_{3L}^{23*} = -0.049 - 0.038i,$ $g_{3L}^{3i} g_{3L}^{23*} = -0.01 - 0.019i$	0.345 ± 0.011	1.037
U_3	1	$h_{3L}^{23} h_{3L}^{33*} = -0.032 - 0.014i,$ $h_{3L}^{2i} h_{3L}^{33*} = 0.003 + 0.002i$	0.349 ± 0.011	1.047
U_3	2	$h_{3L}^{23} h_{3L}^{33*} = -0.014 - 0.006i,$ $h_{3L}^{2i} h_{3L}^{33*} = 0.017 - 0.007i$	0.340 ± 0.010	1.022

Table 6. The values of the $R(\Lambda_c)$ and $R_{\Lambda_c}^{Ratio}$ ratios for two representative cases of the couplings of the different leptoquark models. Above, the index $i = 1, 2$ denotes the electron and muon neutrinos. The Standard-model value of the ratio is $R(\Lambda_c) = 0.333 \pm 0.010$ [48]. The uncertainties given are due to the $\Lambda_b \rightarrow \Lambda_c$ form factor uncertainties.

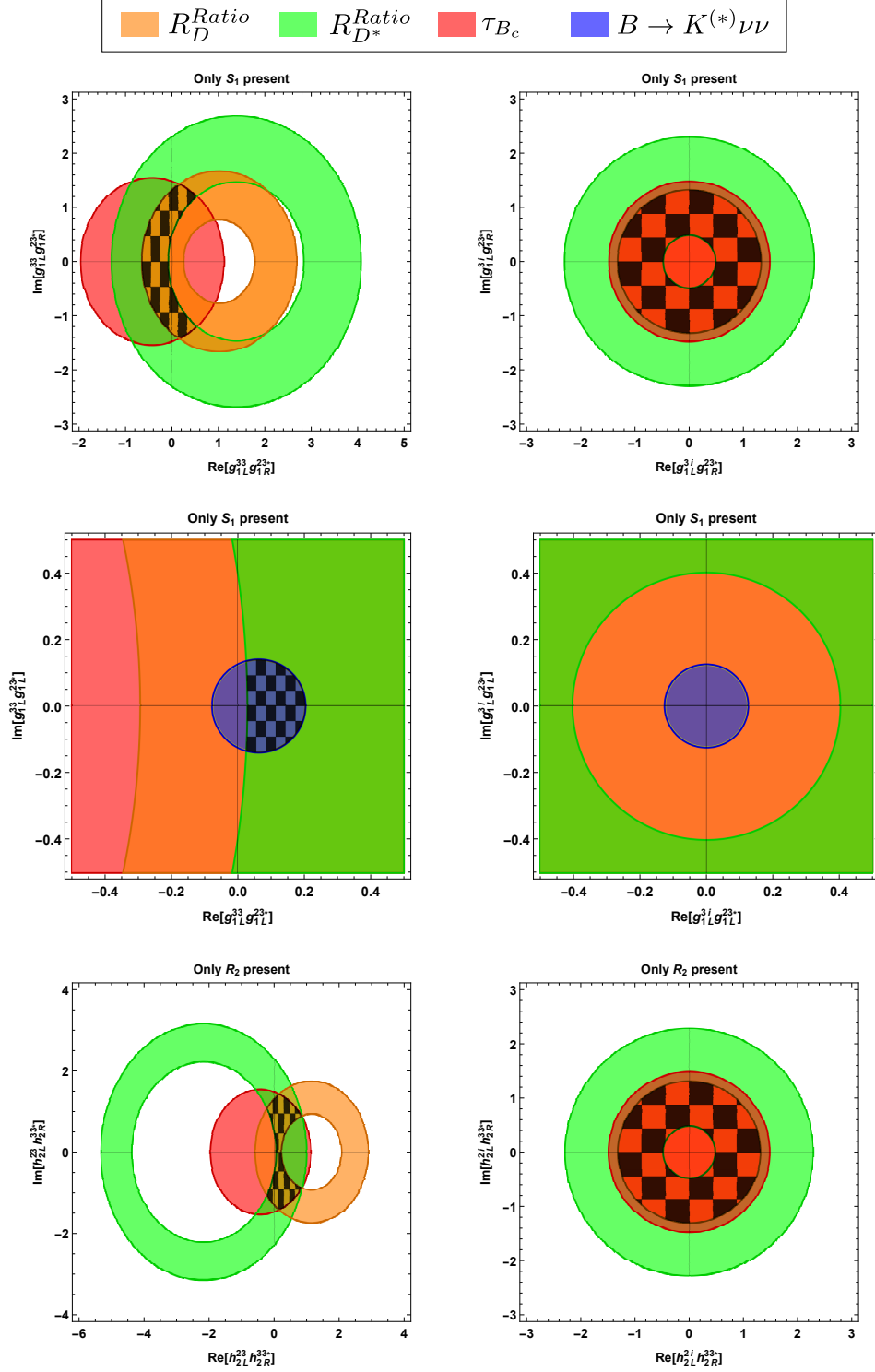


Figure 7. Constraints on the S_1 and R_2 leptoquark models when considering one coupling at a time. Here, $i = 1, 2$ denotes the electron and muon neutrinos. We require that the couplings reproduce the measurements of R_D^{Ratio} and $R_{D^*}^{Ratio}$ in Eqs. (1.7) and (1.8) within 3σ , satisfy $\mathcal{B}(B_c \rightarrow \tau^- \bar{\nu}_\tau) \leq 30\%$, and are consistent with the upper bounds on $\mathcal{B}(B \rightarrow K^{(*)} \nu \bar{\nu})$ at 90% C.L. The allowed regions of the parameter space when combining all constraints are highlighted with a black mesh.

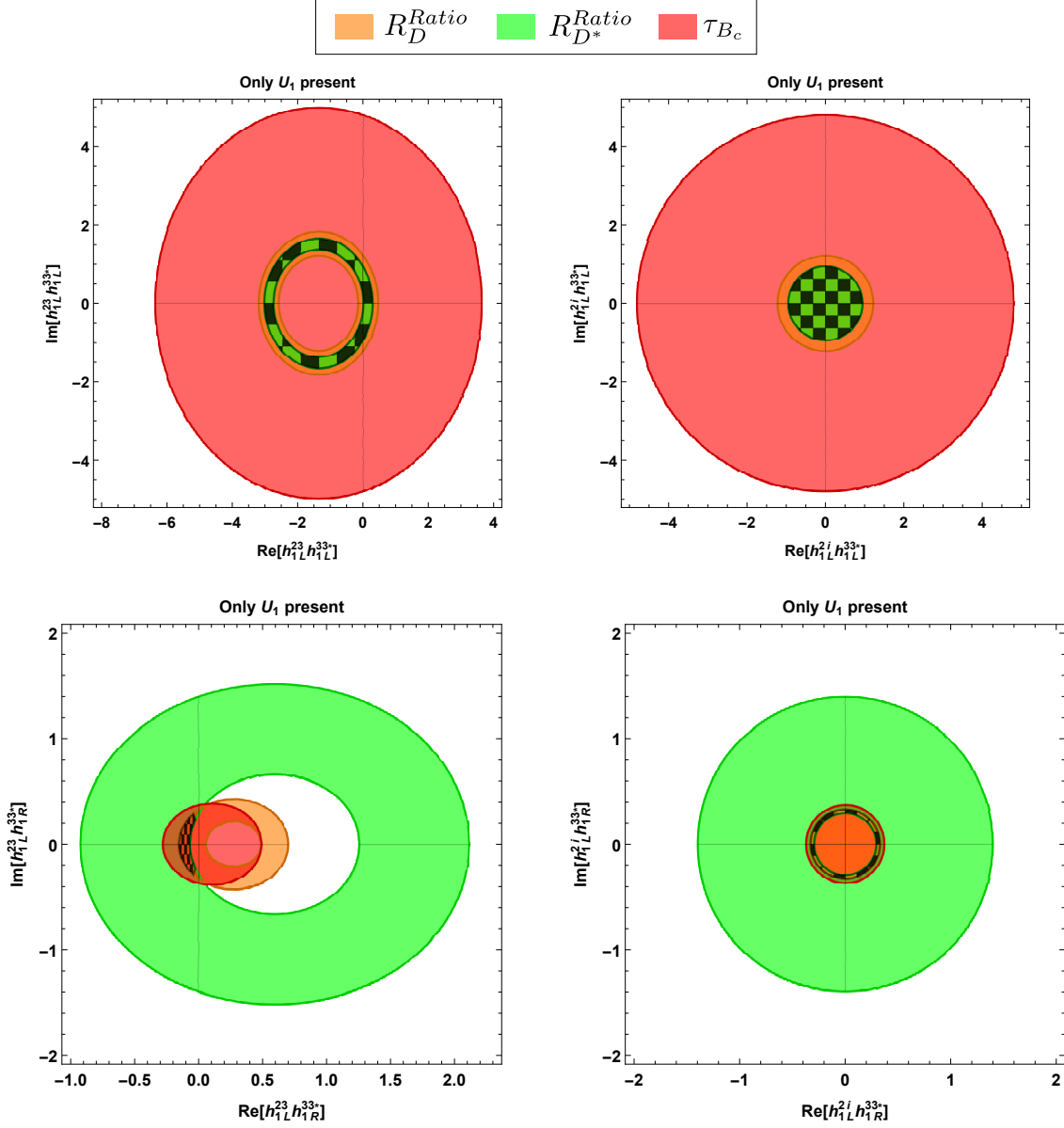


Figure 8. Constraints on the U_1 leptoquark model when considering one coupling at a time. Here, $i = 1, 2$ denotes the electron and muon neutrinos. We require that the couplings reproduce the measurements of R_D^{Ratio} and $R_{D^*}^{Ratio}$ in Eqs. (1.7) and (1.8) within 3σ and satisfy $\mathcal{B}(B_c \rightarrow \tau^- \bar{\nu}_\tau) \leq 30\%$. The allowed regions of the parameter space when combining all constraints are highlighted with a black mesh.

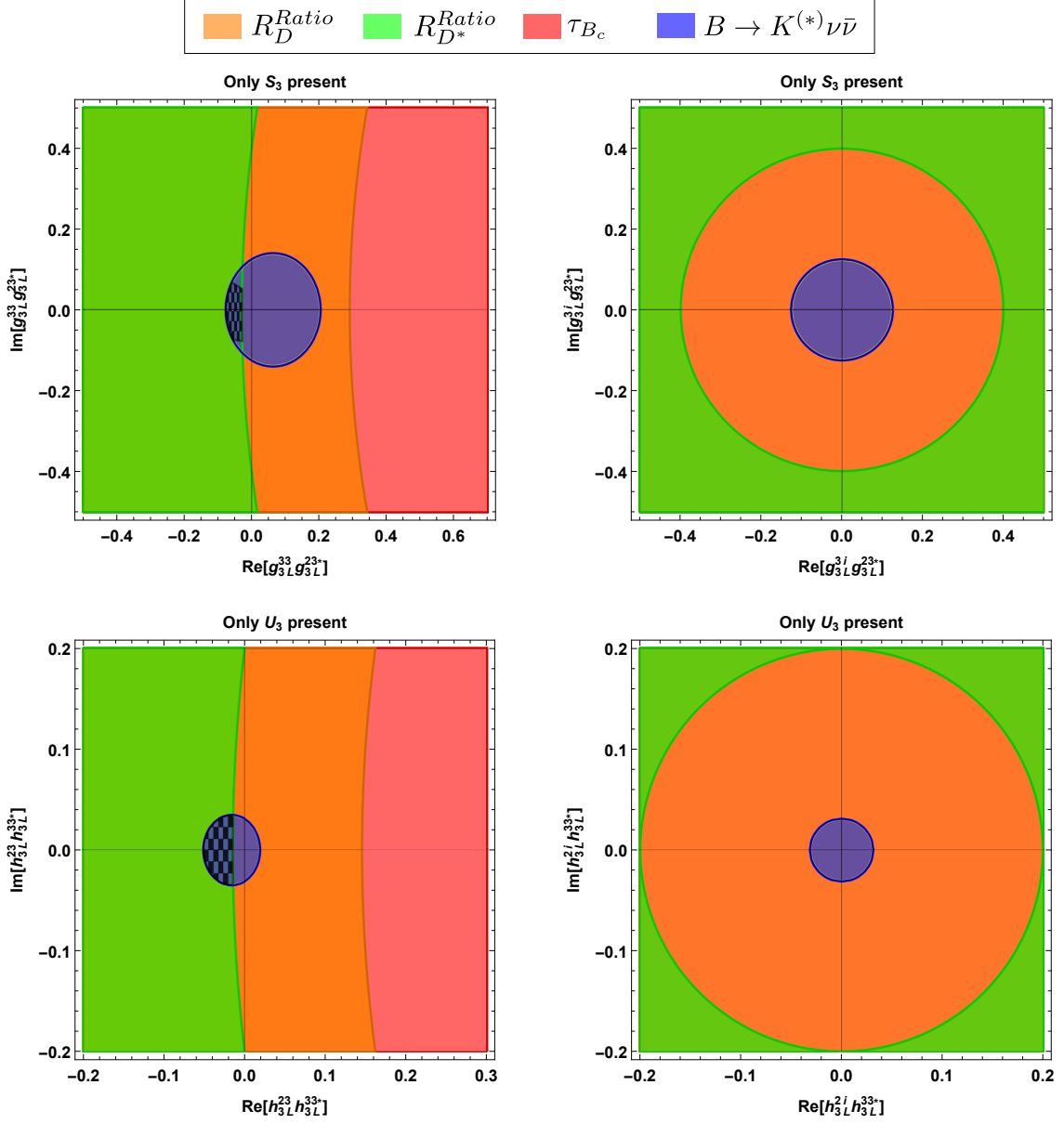


Figure 9. Constraints on the S_3 and U_3 leptoquark models when considering one coupling at a time. Here, $i = 1, 2$ denotes the electron and muon neutrinos. We require that the couplings reproduce the measurements of R_D^{Ratio} and $R_{D^*}^{Ratio}$ in Eqs. (1.7) and (1.8) within 3σ , satisfy $\mathcal{B}(B_c \rightarrow \tau^- \bar{\nu}_\tau) \leq 30\%$, and are consistent with the upper bounds on $\mathcal{B}(B \rightarrow K^{(*)} \nu \bar{\nu})$ at 90% C.L. The allowed regions of the parameter space when combining all constraints are highlighted with a black mesh.

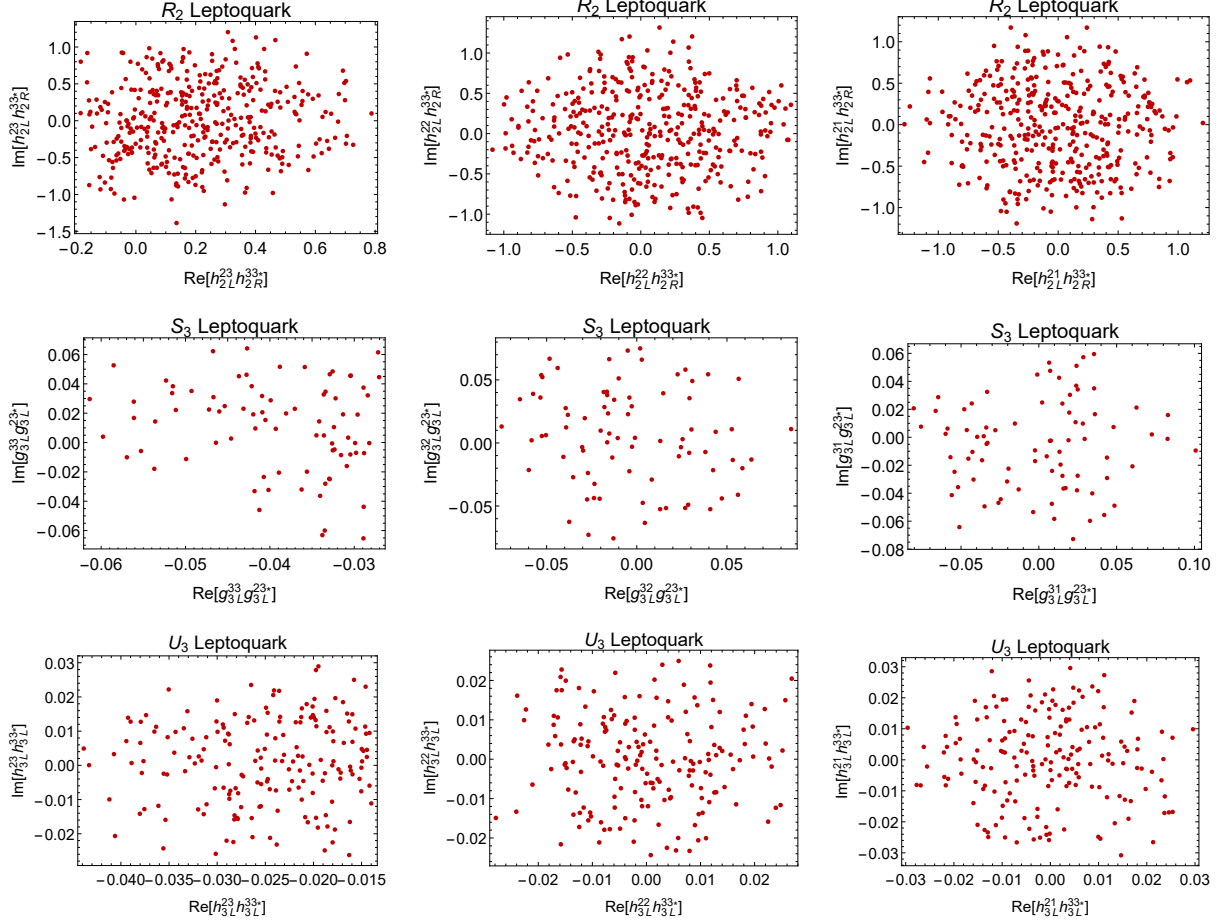


Figure 10. Allowed regions for the couplings of the R_2 , S_3 , and U_3 leptoquark models in the case that all relevant couplings in each model are included simultaneously. We require that the couplings reproduce the measurements of R_D^{Ratio} and $R_{D^*}^{Ratio}$ in Eqs. (1.7) and (1.8) within 3σ , satisfy $\mathcal{B}(B_c \rightarrow \tau^- \bar{\nu}_\tau) \leq 30\%$, and are consistent with the upper bounds on $\mathcal{B}(B \rightarrow K^{(*)} \nu \bar{\nu})$ at 90% C.L (the latter is only relevant for the left-handed couplings in the S_3 and U_3 models).

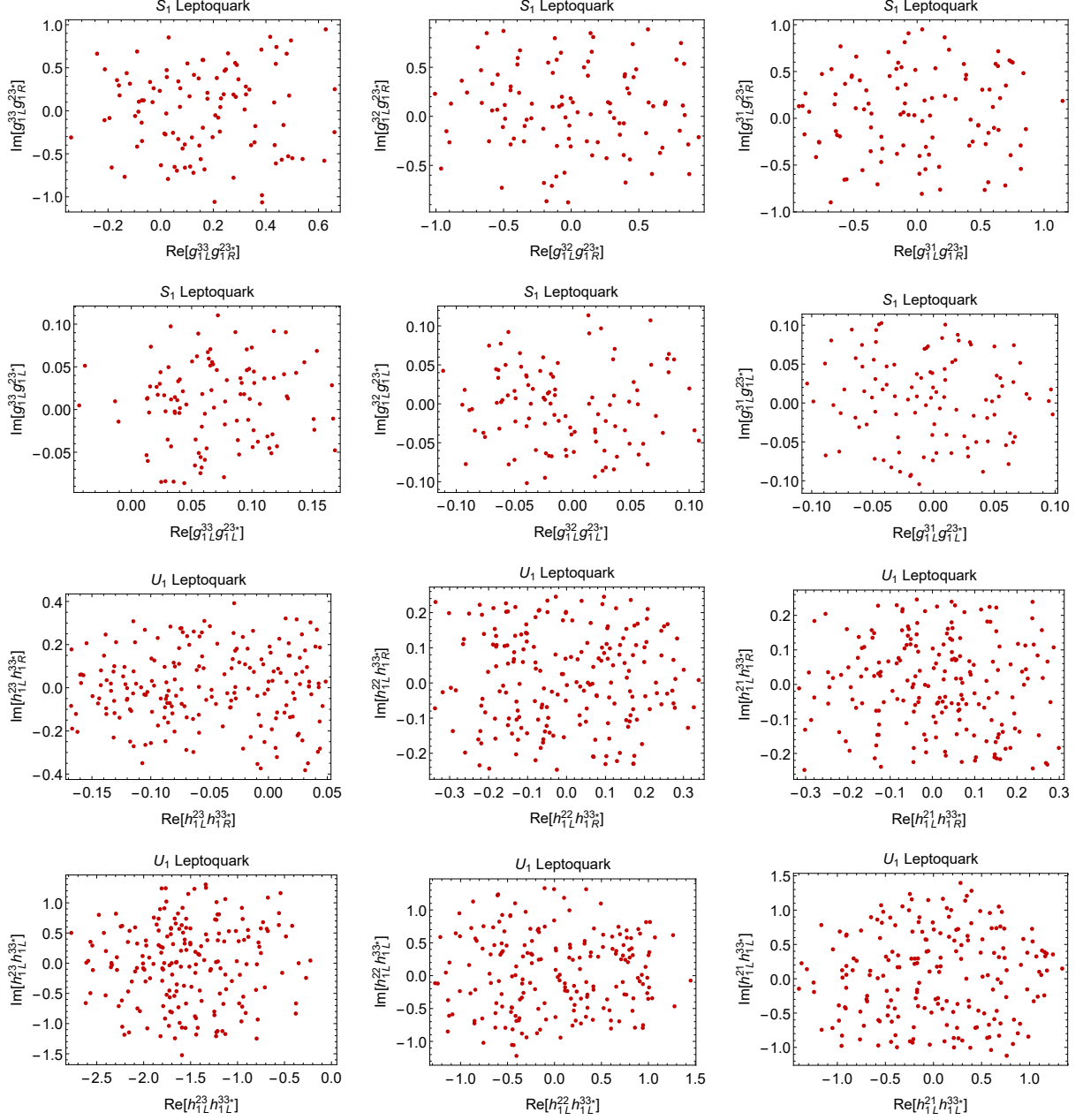


Figure 11. Allowed regions for the couplings of the S_1 and U_1 leptoquark models in the case that all relevant couplings in each model are included simultaneously. We require that the couplings reproduce the measurements of R_D^{Ratio} and $R_{D^*}^{Ratio}$ in Eqs. (1.7) and (1.8) within 3σ , satisfy $\mathcal{B}(B_c \rightarrow \tau^- \bar{\nu}_\tau) \leq 30\%$, and are consistent with the upper bounds on $\mathcal{B}(B \rightarrow K^{(*)} \nu \bar{\nu})$ at 90% C.L (the latter is only relevant for the left-handed couplings in the S_1 model).

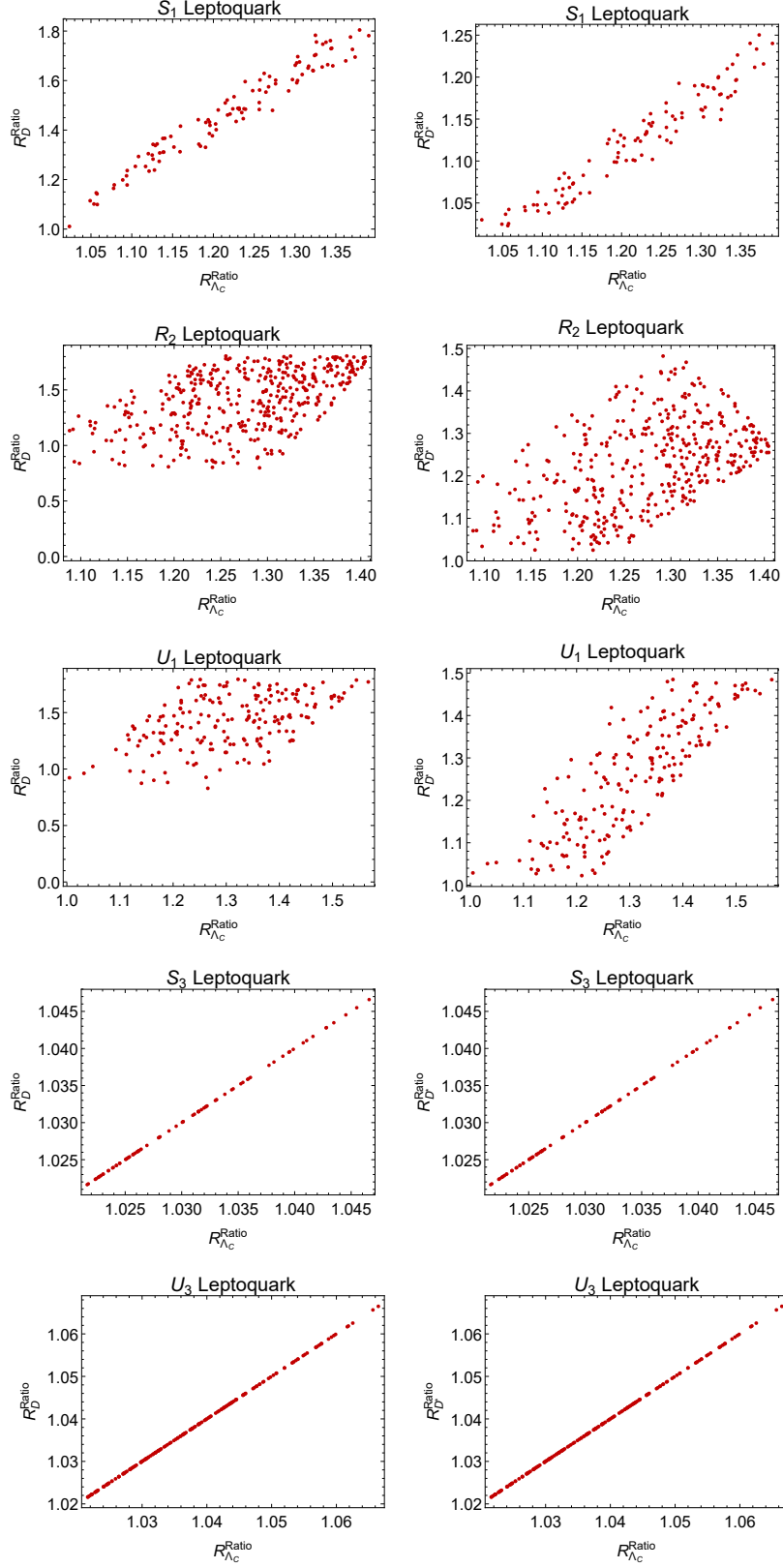


Figure 12. The allowed regions in the $R_{\Lambda_c}^{Ratio} - R_D^{Ratio}$ and $R_{\Lambda_c}^{Ratio} - R_{D^*}^{Ratio}$ planes for each leptoquark model, given the allowed regions for the couplings from Figs. 10 and 11.

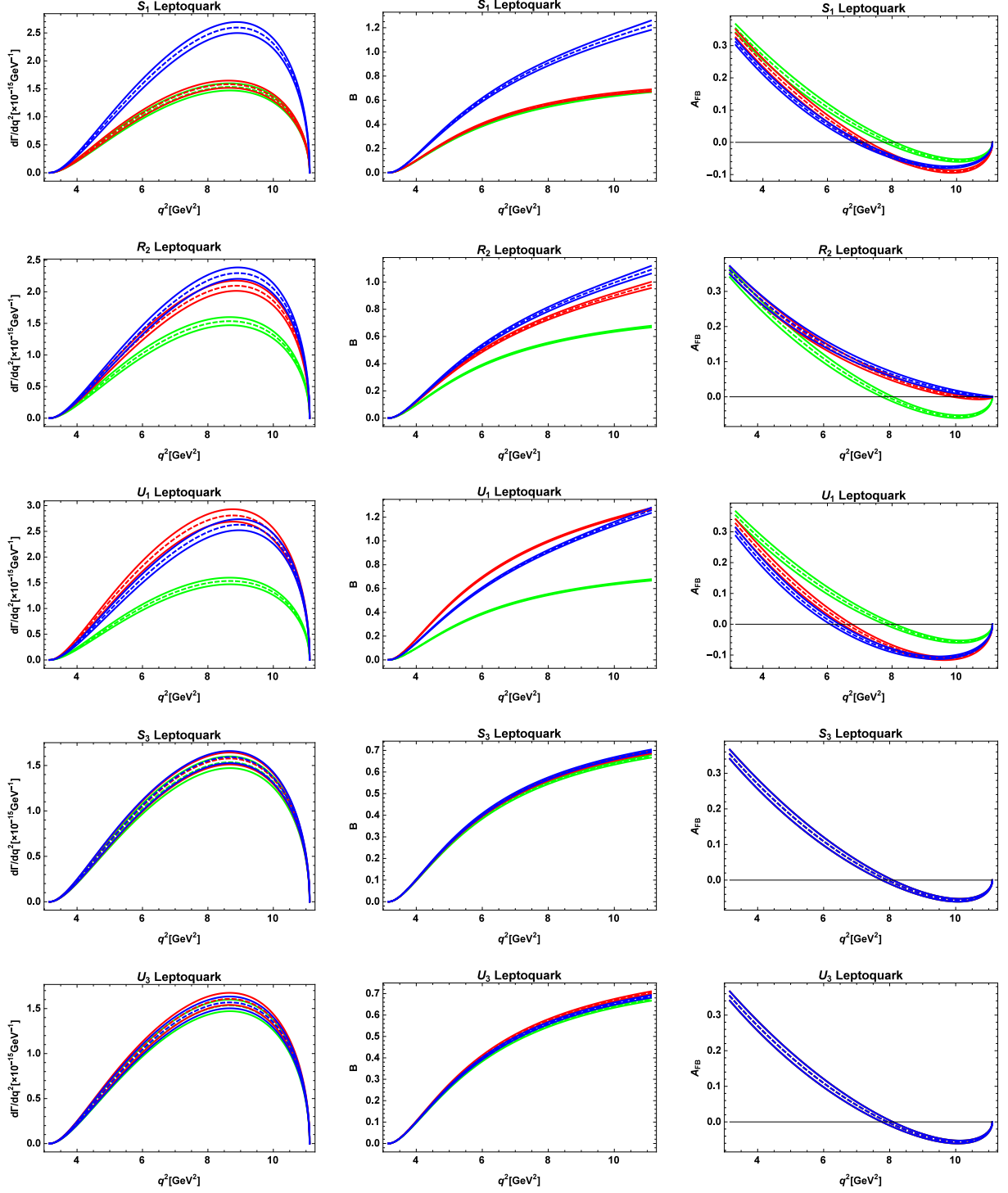


Figure 13. The effects of the different leptoquark models on the $\Lambda_b \rightarrow \Lambda_c \tau \bar{\nu}_\tau$ differential decay rate (left), the ratio of the $\Lambda_b \rightarrow \Lambda_c \tau \bar{\nu}_\tau$ and $\Lambda_b \rightarrow \Lambda_c \ell \bar{\nu}_\ell$ differential decay rates (middle), and the $\Lambda_b \rightarrow \Lambda_c \tau \bar{\nu}_\tau$ forward-backward asymmetry (right), for two representative choices of the couplings. The red and blue curves correspond to the couplings from Cases 1 and 2 in Table 6, respectively, while the green curves correspond to the Standard Model. Because the S_3 and U_3 leptoquarks produce only the vector coupling g_L , the forward-backward asymmetry remains equal to the Standard Model in those cases. The bands indicate the 1σ uncertainties originating from the $\Lambda_b \rightarrow \Lambda_c$ form factors.

6 Conclusions

The baryonic decay $\Lambda_b \rightarrow \Lambda_c \tau \bar{\nu}_\tau$ has the potential to shed new light on the $R(D^{(*)})$ puzzle. Here, we studied the phenomenology of $\Lambda_b \rightarrow \Lambda_c \tau \bar{\nu}_\tau$ in the presence of new-physics couplings with all relevant Dirac structures. In contrast to the mesonic decays, the $\Lambda_b \rightarrow \Lambda_c$ form factors have not yet been determined from experimental data, and it is even more important to use form factors from lattice QCD. Here, we presented new lattice QCD results for the $\Lambda_b \rightarrow \Lambda_c$ tensor form factors, extending the analysis of Ref. [48]. The parameters and covariance matrices of the complete set of $\Lambda_b \rightarrow \Lambda_c$ form factors are provided as supplemental material.

In the first part of our phenomenological analysis, we considered individual new-physics couplings in the effective Hamiltonian in a model-independent way. After constraining these couplings using the $R(D^{(*)})$ measurements and the B_c lifetime, we calculated the effects of the NP couplings in $\Lambda_b \rightarrow \Lambda_c \tau \bar{\nu}_\tau$ decays, focusing on the observables $R(\Lambda_c)$, $B_{\Lambda_c}(q^2)$, and $A_{FB}(q^2)$. Measurements of these observables can help in distinguishing among the different NP operators. For instance, the forward-backward asymmetry $A_{FB}(q^2)$ tends to be mostly above the SM value in the presence of right-handed (g_R) or tensor (g_T) couplings, but is lower than the SM value for most allowed values of the scalar (g_S) coupling. To illustrate the impact of a future $R(\Lambda_c)$ measurement, we presented the constraints on all couplings resulting from two possible ranges of $R(\Lambda_c)$. The baryonic decay can tightly constrain all of the couplings g_L , g_R , g_S , g_P , and g_T . For example, we have shown that if $R_{\Lambda_c}^{Ratio} = R(\Lambda_c)/R(\Lambda_c)^{SM}$ is observed to have a value around 1.3, the scenario with only g_P becomes ruled out by the combined constraints from $R(\Lambda_c)$ and τ_{B_c} .

In the second part of our phenomenological analysis, we considered explicit models in which multiple NP operators are present. For the two-Higgs-doublet model we found significant contribution to $\Lambda_b \rightarrow \Lambda_c \tau \bar{\nu}_\tau$. However, the full numerical analysis was not included in this work as we did not consider RGE evolution which could impact the phenomenology of the model. Models with $SU(2)$ gauge symmetry generally cannot produce large effects in $b \rightarrow c \tau \bar{\nu}_\tau$ transitions without violating bounds from other observables such as B_s mixing, and we therefore did not present their effects on $\Lambda_b \rightarrow \Lambda_c \tau \bar{\nu}_\tau$. On the other hand, we have demonstrated that some of the leptoquark models can produce large effects in the $\Lambda_b \rightarrow \Lambda_c \tau \bar{\nu}_\tau$ observables, in particular through scalar and tensor couplings. We have presented correlation plots of R_D^{Ratio} and $R_{D^*}^{Ratio}$ versus $R_{\Lambda_c}^{Ratio}$, which may be helpful in discriminating among the various models.

Acknowledgments: We thank Shanmuka Shivashankara for early work on this project. This work was financially supported by the National Science Foundation under Grant Nos. PHY-1414345 (AD and AR) and PHY-1520996 (SM). SM is also supported by the RHIC Physics Fellow Program of the RIKEN BNL Research Center. AD acknowledges the hospitality of the Department of Physics and Astronomy, University of Hawaii, where part of the work was done. The lattice QCD calculations were carried out using high-performance computing resources provided by XSEDE (supported by National Science Foundation Grant

No. OCI-1053575) and NERSC (supported by U.S. Department of Energy Grant No. DE-AC02-05CH11231).

A Helicity spinors and polarization vectors

In this appendix, we give explicit expressions for the spinors and polarization vectors used to calculate the helicity amplitudes for the decay $\Lambda_b \rightarrow \Lambda_c \tau \bar{\nu}_\tau$.

A.1 Λ_b rest frame

To calculate the hadronic helicity amplitudes, we work in the Λ_b rest frame and take the three-momentum of the Λ_c along the $+z$ direction and the three-momentum of the virtual vector boson along the $-z$ direction. The baryon spinors are then given by [70]

$$\begin{aligned}\bar{u}_2(\pm\frac{1}{2}, p_{\Lambda_c}) &= \sqrt{E_{\Lambda_c} + m_{\Lambda_c}} \left(\chi_{\pm}^\dagger, \frac{\mp |\mathbf{p}_{\Lambda_c}|}{E_{\Lambda_c} + m_{\Lambda_c}} \chi_{\pm}^\dagger \right), \\ u_1(\pm\frac{1}{2}, p_{\Lambda_b}) &= \sqrt{2m_{\Lambda_b}} \begin{pmatrix} \chi_{\pm} \\ 0 \end{pmatrix},\end{aligned}\tag{A.1}$$

where $\chi_+ = \begin{pmatrix} 1 \\ 0 \end{pmatrix}$ and $\chi_- = \begin{pmatrix} 0 \\ 1 \end{pmatrix}$ are the usual Pauli two-spinors. The polarization vectors of the virtual vector boson are [70]

$$\begin{aligned}\epsilon^{\mu*}(t) &= \frac{1}{\sqrt{q^2}} (q_0; 0, 0, -|\mathbf{q}|), \\ \epsilon^{\mu*}(\pm 1) &= \frac{1}{\sqrt{2}} (0; \pm 1, -i, 0), \\ \epsilon^{\mu*}(0) &= \frac{1}{\sqrt{q^2}} (|\mathbf{q}|; 0, 0, -q_0),\end{aligned}\tag{A.2}$$

where $q^\mu = (q_0; 0, 0, -|\mathbf{q}|)$ is the four-momentum of the virtual vector boson in the Λ_b rest frame. We have

$$q_0 = \frac{1}{2m_{\Lambda_b}} (m_{\Lambda_b}^2 - m_{\Lambda_c}^2 + q^2),\tag{A.3}$$

$$|\mathbf{q}| = |\mathbf{p}_{\Lambda_c}| = \frac{1}{2m_{\Lambda_b}} \sqrt{Q_+ Q_-},\tag{A.4}$$

where

$$Q_{\pm} = (m_{\Lambda_b} \pm m_{\Lambda_c})^2 - q^2.\tag{A.5}$$

A.2 Dilepton rest frame

In the calculation of the lepton helicity amplitudes, we work in the rest frame of the virtual vector boson, which is equal to the rest frame of the $\tau \bar{\nu}_\tau$ dilepton system. We define the angle θ_τ as the angle between the three-momenta of the τ and the Λ_c in this frame.

The lepton spinors for \mathbf{p}_τ pointing in the $+z$ direction and $\mathbf{p}_{\bar{\nu}_\tau}$ pointing in the $-z$ direction are

$$\begin{aligned}\bar{u}_\tau(\pm\frac{1}{2}, p_\tau) &= \sqrt{E_\tau + m_\tau} \left(\chi_{\pm}^\dagger, \frac{\mp |\mathbf{p}_\tau|}{E_\tau + m_\tau} \chi_{\pm}^\dagger \right), \\ v_{\bar{\nu}_\tau}(\frac{1}{2}, p_{\bar{\nu}_\tau}) &= \sqrt{E_\nu} \begin{pmatrix} \chi_+ \\ -\chi_+ \end{pmatrix}.\end{aligned}\tag{A.6}$$

We then rotate about the y axis by the angle θ_τ so that after the rotation, the three-momentum of the Λ_c points in the $+z$ direction. The two-spinors transform as

$$\begin{aligned}\chi'_\pm &= e^{-i\theta_\tau\sigma_2/2}\chi_\pm \\ &= \begin{pmatrix} \cos(\theta_\tau/2) & -\sin(\theta_\tau/2) \\ \sin(\theta_\tau/2) & \cos(\theta_\tau/2) \end{pmatrix} \chi_\pm,\end{aligned}\tag{A.7}$$

and

$$\chi'^\dagger_\pm = \chi^\dagger_\pm \begin{pmatrix} \cos(\theta_\tau/2) & \sin(\theta_\tau/2) \\ -\sin(\theta_\tau/2) & \cos(\theta_\tau/2) \end{pmatrix},\tag{A.8}$$

and the full lepton spinors after the rotation are

$$\begin{aligned}\bar{u}_\tau(+\tfrac{1}{2}, p_\tau) &= \sqrt{E_\tau + m_\tau} \left(\cos(\theta_\tau/2), \sin(\theta_\tau/2), \frac{-|\mathbf{p}_\tau|}{E_\tau + m_\tau} \cos(\theta_\tau/2), \frac{-|\mathbf{p}_\tau|}{E_\tau + m_\tau} \sin(\theta_\tau/2) \right), \\ \bar{u}_\tau(-\tfrac{1}{2}, p_\tau) &= \sqrt{E_\tau + m_\tau} \left(-\sin(\theta_\tau/2), \cos(\theta_\tau/2), \frac{-|\mathbf{p}_\tau|}{E_\tau + m_\tau} \sin(\theta_\tau/2), \frac{|\mathbf{p}_\tau|}{E_\tau + m_\tau} \cos(\theta_\tau/2) \right), \\ v_{\bar{\nu}_\tau}(\tfrac{1}{2}, p_{\bar{\nu}_\tau}) &= \sqrt{E_\nu} \begin{pmatrix} \cos(\theta_\tau/2) \\ \sin(\theta_\tau/2) \\ -\cos(\theta_\tau/2) \\ -\sin(\theta_\tau/2) \end{pmatrix}.\end{aligned}\tag{A.9}$$

The polarization vectors of the virtual vector boson in this frame are

$$\begin{aligned}\epsilon^{\mu*}(t) &= (1; 0, 0, 0), \\ \epsilon^{\mu*}(\pm 1) &= \frac{1}{\sqrt{2}} (0; \pm 1, -i, 0), \\ \epsilon^{\mu*}(0) &= (0; 0, 0, -1).\end{aligned}\tag{A.10}$$

The three-momentum and energy of the τ lepton in this frame can be written as

$$\begin{aligned}|\mathbf{p}_\tau| &= \sqrt{q^2} v^2/2, \\ E_\tau &= |\mathbf{p}_\tau| + m_\tau^2/\sqrt{q^2},\end{aligned}\tag{A.11}$$

where

$$v = \sqrt{1 - \frac{m_\tau^2}{q^2}}.\tag{A.12}$$

References

- [1] BABAR collaboration, J. P. Lees et al., *Measurement of an Excess of $\bar{B} \rightarrow D^{(*)}\tau^-\bar{\nu}_\tau$ Decays and Implications for Charged Higgs Bosons*, *Phys. Rev.* **D88** (2013) 072012, [[1303.0571](#)].
- [2] BELLE collaboration, M. Huschle et al., *Measurement of the branching ratio of $\bar{B} \rightarrow D^{(*)}\tau^-\bar{\nu}_\tau$ relative to $\bar{B} \rightarrow D^{(*)}\ell^-\bar{\nu}_\ell$ decays with hadronic tagging at Belle*, *Phys. Rev.* **D92** (2015) 072014, [[1507.03233](#)].
- [3] BELLE collaboration, A. Abdesselam et al., *Measurement of the branching ratio of $\bar{B}^0 \rightarrow D^{*+}\tau^-\bar{\nu}_\tau$ relative to $\bar{B}^0 \rightarrow D^{*+}\ell^-\bar{\nu}_\ell$ decays with a semileptonic tagging method*, *Phys. Rev. Lett.* **116** (2016) 067111, [[1603.06711](#)].
- [4] LHCb collaboration, R. Aaij et al., *Measurement of the ratio of branching fractions $\mathcal{B}(\bar{B}^0 \rightarrow D^{*+}\tau^-\bar{\nu}_\tau)/\mathcal{B}(\bar{B}^0 \rightarrow D^{*+}\mu^-\bar{\nu}_\mu)$* , *Phys. Rev. Lett.* **115** (2015) 111803, [[1506.08614](#)].
- [5] J. A. Bailey et al., *Refining new-physics searches in $B \rightarrow D\tau\nu$ decay with lattice QCD*, *Phys. Rev. Lett.* **109** (2012) 071802, [[1206.4992](#)].
- [6] MILC collaboration, J. A. Bailey et al., *$B \rightarrow D\ell\nu$ form factors at nonzero recoil and $|V_{cb}|$ from 2+1-flavor lattice QCD*, *Phys. Rev.* **D92** (2015) 034506, [[1503.07237](#)].
- [7] HPQCD collaboration, H. Na, C. M. Bouchard, G. P. Lepage, C. Monahan and J. Shigemitsu, *$B \rightarrow D\ell\nu$ form factors at nonzero recoil and extraction of $|V_{cb}|$* , *Phys. Rev.* **D92** (2015) 054510, [[1505.03925](#)].
- [8] Y. Sakaki, M. Tanaka, A. Tayduganov and R. Watanabe, *Testing leptoquark models in $\bar{B} \rightarrow D^{(*)}\tau\bar{\nu}$* , *Phys. Rev.* **D88** (2013) 094012, [[1309.0301](#)].
- [9] Y.-M. Wang, Y.-B. Wei, Y.-L. Shen and C.-D. Lü, *Perturbative corrections to $B \rightarrow D$ form factors in QCD*, *Phys. Rev. Lett.* **170** (2023) 06810, [[1701.06810](#)].
- [10] S. Fajfer, J. F. Kamenik and I. Nisandzic, *On the $B \rightarrow D^*\tau\bar{\nu}_\tau$ Sensitivity to New Physics*, *Phys. Rev.* **D85** (2012) 094025, [[1203.2654](#)].
- [11] Y. Amhis et al., “Averages of b -hadron, c -hadron, and τ -lepton properties as of winter 2016.” http://www.slac.stanford.edu/xorg/hfag/semi/winter16/winter16_dtaunu.html, 2016.
- [12] G. Ricciardi, *Semileptonic and leptonic B decays, circa 2016*, *Mod. Phys. Lett.* **A32** (2017) 1730005, [[1610.04387](#)].
- [13] C. DeTar, *Private communication*, 2016.
- [14] BABAR collaboration, B. Aubert et al., *Measurement of $|V_{cb}|$ and the Form-Factor Slope in $\bar{B} \rightarrow D^{(*)}\tau\bar{\nu}$ Decays in Events Tagged by a Fully Reconstructed B Meson*, *Phys. Rev. Lett.* **104** (2010) 011802, [[0904.4063](#)].
- [15] BELLE collaboration, R. Glattauer et al., *Measurement of the decay $B \rightarrow D\ell\nu_\ell$ in fully reconstructed events and determination of the Cabibbo-Kobayashi-Maskawa matrix element $|V_{cb}|$* , *Phys. Rev.* **D93** (2016) 032006, [[1510.03657](#)].
- [16] S. Fajfer, J. F. Kamenik, I. Nisandzic and J. Zupan, *Implications of Lepton Flavor Universality Violations in B Decays*, *Phys. Rev. Lett.* **109** (2012) 161801, [[1206.1872](#)].
- [17] A. Crivellin, C. Greub and A. Kokulu, *Explaining $B \rightarrow D\tau\nu$, $B \rightarrow D^*\tau\nu$ and $B \rightarrow \tau\nu$ in a 2HDM of type III*, *Phys. Rev.* **D86** (2012) 054014, [[1206.2634](#)].
- [18] A. Datta, M. Duraisamy and D. Ghosh, *Diagnosing New Physics in $b \rightarrow c\tau\nu_\tau$ decays in the light of the recent BaBar result*, *Phys. Rev.* **D86** (2012) 034027, [[1206.3760](#)].

- [19] D. Becirevic, N. Kosnik and A. Tayduganov, $\bar{B} \rightarrow D\tau\bar{\nu}_\tau$ vs. $\bar{B} \rightarrow D\mu\bar{\nu}_\mu$, *Phys. Lett.* **B716** (2012) 208–213, [[1206.4977](#)].
- [20] N. G. Deshpande and A. Menon, *Hints of R-parity violation in B decays into $\tau\nu$* , *JHEP* **01** (2013) 025, [[1208.4134](#)].
- [21] A. Celis, M. Jung, X.-Q. Li and A. Pich, *Sensitivity to charged scalars in $B \rightarrow D^{(*)}\tau\nu_\tau$ and $B \rightarrow \tau\nu_\tau$ decays*, *JHEP* **01** (2013) 054, [[1210.8443](#)].
- [22] D. Choudhury, D. K. Ghosh and A. Kundu, *B decay anomalies in an effective theory*, *Phys. Rev.* **D86** (2012) 114037, [[1210.5076](#)].
- [23] M. Tanaka and R. Watanabe, *New physics in the weak interaction of $\bar{B} \rightarrow D^{(*)}\tau\bar{\nu}$* , *Phys. Rev.* **D87** (2013) 034028, [[1212.1878](#)].
- [24] P. Ko, Y. Omura and C. Yu, *$B \rightarrow D^{(*)}\tau\nu$ and $B \rightarrow \tau\nu$ in chiral $U(1)'$ models with flavored multi Higgs doublets*, *JHEP* **03** (2013) 151, [[1212.4607](#)].
- [25] Y.-Y. Fan, W.-F. Wang, S. Cheng and Z.-J. Xiao, *Semileptonic decays $B \rightarrow D^{(*)}l\nu$ in the perturbative QCD factorization approach*, *Chin. Sci. Bull.* **59** (2014) 125–132, [[1301.6246](#)].
- [26] P. Biancofiore, P. Colangelo and F. De Fazio, *On the anomalous enhancement observed in $B \rightarrow D^{(*)}\tau\bar{\nu}_\tau$ decays*, *Phys. Rev.* **D87** (2013) 074010, [[1302.1042](#)].
- [27] A. Celis, M. Jung, X.-Q. Li and A. Pich, *$B \rightarrow D^{(*)}\tau\bar{\nu}_\tau$ decays in two-Higgs-doublet models*, *J. Phys. Conf. Ser.* **447** (2013) 012058, [[1302.5992](#)].
- [28] M. Duraisamy and A. Datta, *The Full $B \rightarrow D^*\tau^-\bar{\nu}_\tau$ Angular Distribution and CP violating Triple Products*, *JHEP* **09** (2013) 059, [[1302.7031](#)].
- [29] I. Dorsner, S. Fajfer, N. Kosnik and I. Nisandzic, *Minimally flavored colored scalar in $\bar{B} \rightarrow D^{(*)}\tau\bar{\nu}$ and the mass matrices constraints*, *JHEP* **11** (2013) 084, [[1306.6493](#)].
- [30] Y. Sakaki, M. Tanaka, A. Tayduganov and R. Watanabe, *Probing New Physics with q^2 distributions in $\bar{B} \rightarrow D^{(*)}\tau\bar{\nu}$* , *Phys. Rev.* **D91** (2015) 114028, [[1412.3761](#)].
- [31] B. Bhattacharya, A. Datta, D. London and S. Shivashankara, *Simultaneous Explanation of the R_K and $R(D^{(*)})$ Puzzles*, *Phys. Lett.* **B742** (2015) 370–374, [[1412.7164](#)].
- [32] LHCb collaboration, R. Aaij et al., *Test of lepton universality using $B^+ \rightarrow K^+\ell^+\ell^-$ decays*, *Phys. Rev. Lett.* **113** (2014) 151601, [[1406.6482](#)].
- [33] LHCb collaboration, R. Aaij et al., *Measurement of Form-Factor-Independent Observables in the Decay $B^0 \rightarrow K^{*0}\mu^+\mu^-$* , *Phys. Rev. Lett.* **111** (2013) 191801, [[1308.1707](#)].
- [34] LHCb collaboration, R. Aaij et al., *Angular analysis of the $B^0 \rightarrow K^{*0}\mu^+\mu^-$ decay using 3 fb^{-1} of integrated luminosity*, *JHEP* **02** (2016) 104, [[1512.04442](#)].
- [35] T. Blake, G. Lanfranchi and D. M. Straub, *Rare B Decays as Tests of the Standard Model*, *Prog. Part. Nucl. Phys.* **92** (2017) 50–91, [[1606.00916](#)].
- [36] L. Calibbi, A. Crivellin and T. Ota, *Effective Field Theory Approach to $b \rightarrow s\ell\ell^{(\prime)}$, $B \rightarrow K^{(*)}\nu\bar{\nu}$ and $B \rightarrow D^{(*)}\tau\nu$ with Third Generation Couplings*, *Phys. Rev. Lett.* **115** (2015) 181801, [[1506.02661](#)].
- [37] A. Greljo, G. Isidori and D. Marzocca, *On the breaking of Lepton Flavor Universality in B decays*, *JHEP* **07** (2015) 142, [[1506.01705](#)].
- [38] S. M. Boucenna, A. Celis, J. Fuentes-Martin, A. Vicente and J. Virto, *Non-abelian gauge extensions for B-decay anomalies*, *Phys. Lett.* **B760** (2016) 214–219, [[1604.03088](#)].

- [39] B. Bhattacharya, A. Datta, J.-P. Guevin, D. London and R. Watanabe, *Simultaneous Explanation of the R_K and $R_{D^{(*)}}$ Puzzles: a Model Analysis*, *JHEP* **01** (2017) 015, [[1609.09078](#)].
- [40] R. Barbieri, C. W. Murphy and F. Senia, *B-decay Anomalies in a Composite Leptoquark Model*, *Eur. Phys. J.* **C77** (2017) 8, [[1611.04930](#)].
- [41] T. Gutsche, M. A. Ivanov, J. G. Korner, V. E. Lyubovitskij, P. Santorelli and N. Habył, *Semileptonic decay $\Lambda_b \rightarrow \Lambda_c + \tau^- + \bar{\nu}_\tau$ in the covariant confined quark model*, *Phys. Rev.* **D91** (2015) 074001, [[1502.04864](#)].
- [42] R. M. Woloshyn, *Semileptonic decay of the Λ_b baryon*, *PoS Hadron2013* (2013) 203.
- [43] S. Shivashankara, W. Wu and A. Datta, *$\Lambda_b \rightarrow \Lambda_c \tau \bar{\nu}_\tau$ Decay in the Standard Model and with New Physics*, *Phys. Rev.* **D91** (2015) 115003, [[1502.07230](#)].
- [44] R. Dutta, *$\Lambda_b \rightarrow (\Lambda_c, p) \tau \nu$ decays within standard model and beyond*, *Phys. Rev.* **D93** (2016) 054003, [[1512.04034](#)].
- [45] R. N. Faustov and V. O. Galkin, *Semileptonic decays of Λ_b baryons in the relativistic quark model*, *Phys. Rev.* **D94** (2016) 073008, [[1609.00199](#)].
- [46] X.-Q. Li, Y.-D. Yang and X. Zhang, *$\Lambda_b \rightarrow \Lambda_c \tau \bar{\nu}_\tau$ decay in scalar and vector leptoquark scenarios*, [1611.01635](#).
- [47] A. Celis, M. Jung, X.-Q. Li and A. Pich, *Scalar contributions to $b \rightarrow c(u) \tau \nu$ transitions*, [1612.07757](#).
- [48] W. Detmold, C. Lehner and S. Meinel, *$\Lambda_b \rightarrow p \ell^- \bar{\nu}_\ell$ and $\Lambda_b \rightarrow \Lambda_c \ell^- \bar{\nu}_\ell$ form factors from lattice QCD with relativistic heavy quarks*, *Phys. Rev.* **D92** (2015) 034503, [[1503.01421](#)].
- [49] X.-Q. Li, Y.-D. Yang and X. Zhang, *Revisiting the one leptoquark solution to the $R(D^0)$ anomalies and its phenomenological implications*, *JHEP* **08** (2016) 054, [[1605.09308](#)].
- [50] R. Alonso, B. Grinstein and J. Martin Camalich, *The lifetime of the B_c^- meson and the anomalies in $B \rightarrow D^{(*)} \tau \nu$* , [1611.06676](#).
- [51] C.-H. Chen and C.-Q. Geng, *Lepton angular asymmetries in semileptonic charmful B decays*, *Phys. Rev.* **D71** (2005) 077501, [[hep-ph/0503123](#)].
- [52] T. Bhattacharya, V. Cirigliano, S. D. Cohen, A. Filipuzzi, M. Gonzalez-Alonso, M. L. Graesser et al., *Probing Novel Scalar and Tensor Interactions from (Ultra)Cold Neutrons to the LHC*, *Phys. Rev.* **D85** (2012) 054512, [[1110.6448](#)].
- [53] F. Feruglio, P. Paradisi and A. Pattori, *Revisiting Lepton Flavor Universality in B Decays*, *Phys. Rev. Lett.* **118** (2017) 011801, [[1606.00524](#)].
- [54] F. Feruglio, P. Paradisi and A. Pattori, *On the Importance of Electroweak Corrections for B Anomalies*, [1705.00929](#).
- [55] T. Feldmann and M. W. Y. Yip, *Form Factors for $\Lambda_b \rightarrow \Lambda$ Transitions in SCET*, *Phys. Rev.* **D85** (2012) 014035, [[1111.1844](#)].
- [56] PARTICLE DATA GROUP collaboration, C. Patrignani et al., *Review of Particle Physics*, *Chin. Phys.* **C40** (2016) 100001.
- [57] W. Detmold and S. Meinel, *$\Lambda_b \rightarrow \Lambda \ell^+ \ell^-$ form factors, differential branching fraction, and angular observables from lattice QCD with relativistic b quarks*, *Phys. Rev.* **D93** (2016) 074501, [[1602.01399](#)].

- [58] C. Bourrely, I. Caprini and L. Lellouch, *Model-independent description of $B \rightarrow \pi \ell \nu$ decays and a determination of $|V_{ub}|$* , *Phys. Rev.* **D79** (2009) 013008, [[0807.2722](#)].
- [59] A. Abdesselam et al., *Measurement of the τ lepton polarization in the decay $\bar{B} \rightarrow D^* \tau^- \bar{\nu}_\tau$* , *Phys. Rev. Lett.* **1608.06391**.
- [60] M. Beneke and G. Buchalla, *The B_c Meson Lifetime*, *Phys. Rev.* **D53** (1996) 4991–5000, [[hep-ph/9601249](#)].
- [61] HPQCD collaboration, B. Colquhoun, C. T. H. Davies, R. J. Dowdall, J. Kettle, J. Koponen, G. P. Lepage et al., *B-meson decay constants: a more complete picture from full lattice QCD*, *Phys. Rev.* **D91** (2015) 114509, [[1503.05762](#)].
- [62] R. Alonso, B. Grinstein and J. Martin Camalich, *Lepton universality violation and lepton flavor conservation in B-meson decays*, *JHEP* **10** (2015) 184, [[1505.05164](#)].
- [63] P. M. Ferreira, L. Lavoura and J. P. Silva, *Renormalization-group constraints on Yukawa alignment in multi-Higgs-doublet models*, *Phys. Lett.* **B688** (2010) 341–344, [[1001.2561](#)].
- [64] A. Pich and P. Tuzon, *Yukawa Alignment in the Two-Higgs-Doublet Model*, *Phys. Rev.* **D80** (2009) 091702, [[0908.1554](#)].
- [65] B. Dumont, K. Nishiwaki and R. Watanabe, *LHC constraints and prospects for S_1 scalar leptoquark explaining the $\bar{B} \rightarrow D^{(*)} \tau \bar{\nu}$ anomaly*, *Phys. Rev.* **D94** (2016) 034001, [[1603.05248](#)].
- [66] BABAR collaboration, J. P. Lees et al., *Search for $B \rightarrow K^{(*)} \nu \bar{\nu}$ and invisible quarkonium decays*, *Phys. Rev.* **D87** (2013) 112005, [[1303.7465](#)].
- [67] BELLE collaboration, O. Lutz et al., *Search for $B \rightarrow h^{(*)} \nu \bar{\nu}$ with the full Belle $\Upsilon(4S)$ data sample*, *Phys. Rev.* **D87** (2013) 111103, [[1303.3719](#)].
- [68] A. J. Buras, J. Girrbach-Noe, C. Niehoff and D. M. Straub, *$B \rightarrow K^{(*)} \nu \bar{\nu}$ decays in the Standard Model and beyond*, *JHEP* **02** (2015) 184, [[1409.4557](#)].
- [69] A. J. Buras, *Weak Hamiltonian, CP violation and rare decays*, in *Probing the standard model of particle interactions. Proceedings, Summer School in Theoretical Physics, NATO Advanced Study Institute, 68th session, Les Houches, France, July 28-September 5, 1997. Pt. 1, 2*, pp. 281–539, 1998. [[hep-ph/9806471](#)].
- [70] P. R. Auvil and J. J. Brehm, *Wave Functions for Particles of Higher Spin*, *Phys. Rev.* **145** (1966) 1152.